We are IntechOpen,
the world's leading publisher of
Open Access books
Built by scientists, for scientists

6,900
Open access books available

185,000
International authors and editors

200M
Downloads

154
Countries delivered to

Our authors are among the

TOP 1%
most cited scientists

12.2%
Contributors from top 500 universities

CLARIVATE ANALYTICS

BOOK CITATION INDEX

INDEXED

WEB OF SCIENCE™

Selection of our books indexed in the Book Citation Index
in Web of Science™ Core Collection (BKCI)

Interested in publishing with us?
Contact book.department@intechopen.com

Numbers displayed above are based on latest data collected.
For more information visit www.intechopen.com

Prediction of Typical Beach Changes Owing to Human Activities

Takaaki Uda, Masumi Serizawa and Shiho Miyahara

Abstract

Beach changes related to human activities, such as the effect of construction of groynes and detached breakwaters on a coast with prevailing longshore sand transport, and offshore sand mining, which have engineering importance, were predicted using the Types 1 and 2 BG model. When a long port breakwater is extended, a large wave-shelter zone is formed and dominant longshore sand transport is induced from outside to inside the wave-shelter zone, resulting erosion outside the wave-shelter zone and accretion inside the wave-shelter zone. These beach changes were also predicted using the Type 2 BG model with the evaluation of the effect of a jetty extended at the port entrance to reduce sand deposition inside the port.

Keywords: beach changes, groynes, detached breakwater, offshore sand mining, port breakwater, wave-shelter zone, longshore sand transport

1. Introduction

Beach changes triggered by human activities, such as the construction of groynes and detached breakwaters as a measure against beach erosion, dredging in navigation channel, and offshore sand mining, have been predicted using the Type 1 BG model in previous papers [1–3]. Also, beach changes on the nearby coast triggered by the repeated dredging operation of the anchorage ground in a port were calculated in [1–3]. These results described are commonly observed on many coasts and important in practical coastal engineering, so that these issues were studied again in this chapter by the numerical simulations using the Types 1 and 2 BG model.

Groynes have been used for a long time as one of the most common measures to build statically or dynamically stable shoreline by reducing longshore sand transport on a coast with prevailing longshore sand transport. The effect of the groynes in controlling longshore sand transport strongly depends upon its point depth h in comparison with the depth of closure h_c. If h is greater than h_c, almost all longshore sand transport is blocked, whereas if h is smaller than h_c, a part of longshore sand transport can be transported downcoast, turning around the tip of the groyne. The effect of the construction of the groynes, therefore, was investigated in Section 2 using the Type 1 BG model on a coast with prevailing longshore sand transport under the condition that h is smaller than h_c, which permits passage of part of longshore sand transport offshore of the groynes.

Detached breakwaters have also been widely employed in Japan as one of the measures against beach erosion. Normally, detached breakwaters have been constructed to reduce the wave energy reaching the shoreline, and wave dissipation by the offshore breakwaters will induce sand accumulation behind the detached breakwaters, resulting in the formation of a cuspate foreland. In such a condition, longshore sand transport is induced from outside to inside the wave-shelter zone as a result of the formation of a wave-shelter zone, resulting in erosion outside the wave-shelter zone and accretion inside the wave-shelter zone [1, 3]. This induced longshore sand transport owing to the wave-sheltering effect of the breakwater can be evaluated by Ozasa and Brampton's method [4], in which an additional term of longshore sand transport owing to the longshore change in the breaker height is included as in Type 2 BG model. Moreover, when they are constructed on a coast with prevailing longshore sand transport, often severe downcoast erosion occurs. Therefore, the difference in the effect of the construction of the detached breakwaters was investigated in Section 3 using the Type 2 BG model when waves were incident from the direction normal to the shoreline and obliquely incident.

In the past, offshore sand mining has been extensively carried out in Japan, particularly in the Western Japan, which triggered beach erosion in the vicinity of the offshore holes produced by sand mining [1]. The offshore mining in the depth zone, the depth of which is comparable to the depth of closure, exerts significant impact to the nearby coasts. Such beach changes can be also predicted using the Type 1 BG model. The impact of the offshore sand mining to the nearby coast and sand dune was numerically predicted in Section 4.

In the coastal zone development, a long breakwater of the commercial or fishing port has been constructed at many coasts, forming a large wave-shelter zone on the lee of the offshore breakwater. In this case, beach changes inside and outside the wave-shelter zone of an oblique port breakwater are triggered, similarly to the case of detached breakwaters. These beach changes were predicted in Section 5 using the Type 2 BG model.

When a long port breakwater is extended, longshore sand transport from outside the wave-shelter zone to inside the wave-shelter zone occurs, and sand refills in the navigation channel. The ordinary way for maintaining the channel is the dredging. However, the repetition of the dredging operation of the navigation channel accelerates sand loss on the nearby coast, unless dredged sand is returned to the beach. In the previous work [1], this issue was analyzed using the Type 1 BG model. In Section 6, the mechanism of sand deposition inside the wave-shelter zone after the overall dredging inside the port was predicted by Type 2 BG model, and the effect of a jetty preventing sand from depositing inside the port was predicted.

2. Beach changes around groynes

2.1 Calculation conditions

A calculation domain of 2000 m length and 600 m width in the longshore and cross-shore directions, respectively, was adopted. Assume that two impermeable groynes were installed at an interval of 500 m on a straight coast with the parallel contours and the initial slope of 1/20 and that waves were obliquely incident relative to the normal to the initial shoreline at a breaker angle of 10° (**Figure 1(a)**). The point depth of two groynes, the berm height h_R, and the depth of closure h_c were assumed to be 5, 3, and 10 m, respectively. The point depth (5 m) of the groynes is smaller than the depth of closure, so that part of littoral drift can turn around the tip of the groynes. As the incident waves, waves with a breaker height of $H_b = 3$ m were assumed, and this breaker height was given at each point in the calculation
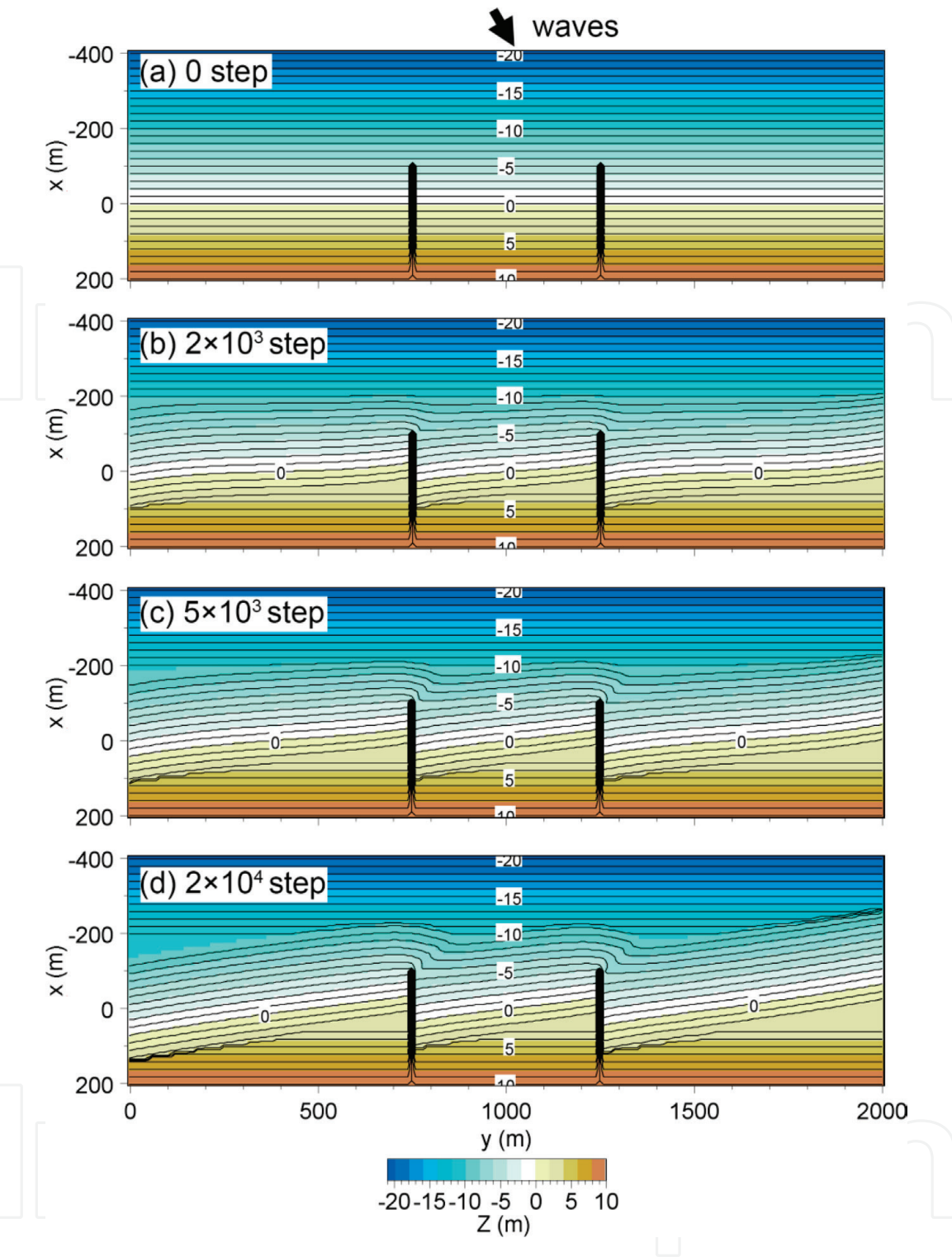
Figure 1.
Prediction of topographic changes around two groynes installed on coast with parallel contours under oblique wave incidence.

domain. The equilibrium slope was the same as the initial slope of $\tan\beta_c = 1/20$. The numerical calculation was carried out using the Type 1 BG model. The other calculation conditions, such as the coefficients of sand transport, mesh size, time intervals, and boundary conditions, are summarized in **Table 1**.

2.2 Calculation results

Subsequent topographic changes and sand transport flux around two groynes installed on a coast with parallel contours under oblique wave incidence are shown in **Figures 1** and **2**. By 2×10^3 steps, the contours upcoast (downcoast) of the groynes advanced (receded) owing to the longshore sand transport toward the positive

Calculation methods	Type 1 BG model
Wave conditions	Incident waves: H_b = 3 m, wave direction θ_w = 10°
Berm height	h_R = 3 m
Depth of closure	h_c = 10 m
Equilibrium slope	$\tan\beta_c$ = 1/20
Depth distribution of sand transport	Cubic equation (Uda and Kawano [5])
Angle of repose slope	$\tan\beta_g$ = 1/2
Coefficients of sand transport	Coefficient of longshore and cross-shore sand transport K_1 = 0.2 Coefficient of Ozasa and Brampton [4] term K_2 = 0.0
Mesh size	$\Delta x = \Delta y$ = 10 m
Time intervals	Δt = 0.05 h
Duration of calculation	1.5×10^3 h (3×10^4 steps)
Boundary conditions	Shoreward and landward ends q_x = 0 Right and left boundaries q_y = 0
Remarks	Lower minimum of 0.5 was set for $|\cos\alpha_b|$ in calculation of P value (Eq. (4) in Chap. 2) to avoid local discontinuity in topography

Table 1.
Calculation conditions.

y-direction (**Figure 1(b)**). Because the groyne insufficiently blocked rightward longshore sand transport, part of longshore sand transport turned around the tip of the groynes, as shown in **Figure 2(a)**, resulting in meandering of offshore contours (**Figure 1(b)**). With time, the meandering of contours offshore of the groynes became more prominent, whereas parallel contours were formed between the groynes as well as the formation of a scarp downcoast of the groynes (**Figure 1(c)** and **(d)**). The sand transport flux offshore of the tip of the groyne still continues after 5×10^3 and 2×10^4 steps with gradual decrease in the intensity. In the meantime, the accretion and erosion zones upcoast and downcoast of the groyne, respectively, expanded, as shown in **Figure 2(b)** and **(c)**. These topographic changes between the groynes including the meandering of contours offshore of the groynes are commonly observed in the field or in a movable bed experiment [1, 3], and such characteristics were successfully reproduced by the Type 1 BG model. **Figure 3** shows the shoreline changes around two groynes. The straight shoreline at the initial stage changed stepwise with time, and the shoreline was stabilized so as for the shoreline to be normal to the wave direction.

The prediction of the meandering of offshore contours became possible only if a stabilization mechanism of the longitudinal profile is taken into account. **Figure 4** shows a schematic diagram of sand transport in the vicinity of a groyne. Consider two contours with the depths h_1 and h_2 and that the cross-shore distance between h_1 and h_2 is a. In addition, consider the extension of a groyne with a point depth between h_1 and h_2, and assume that the shoreward contour advances or retreats by b upcoast and downcoast of the groyne, respectively. If the seabed slope in the longitudinal profile was equal to the equilibrium slope before the beach changes, we obtain the relations for the equilibrium slope and the beach slope after the beach changes:

$$\tan\beta_c = (h_2 - h_1)/a \tag{1}$$
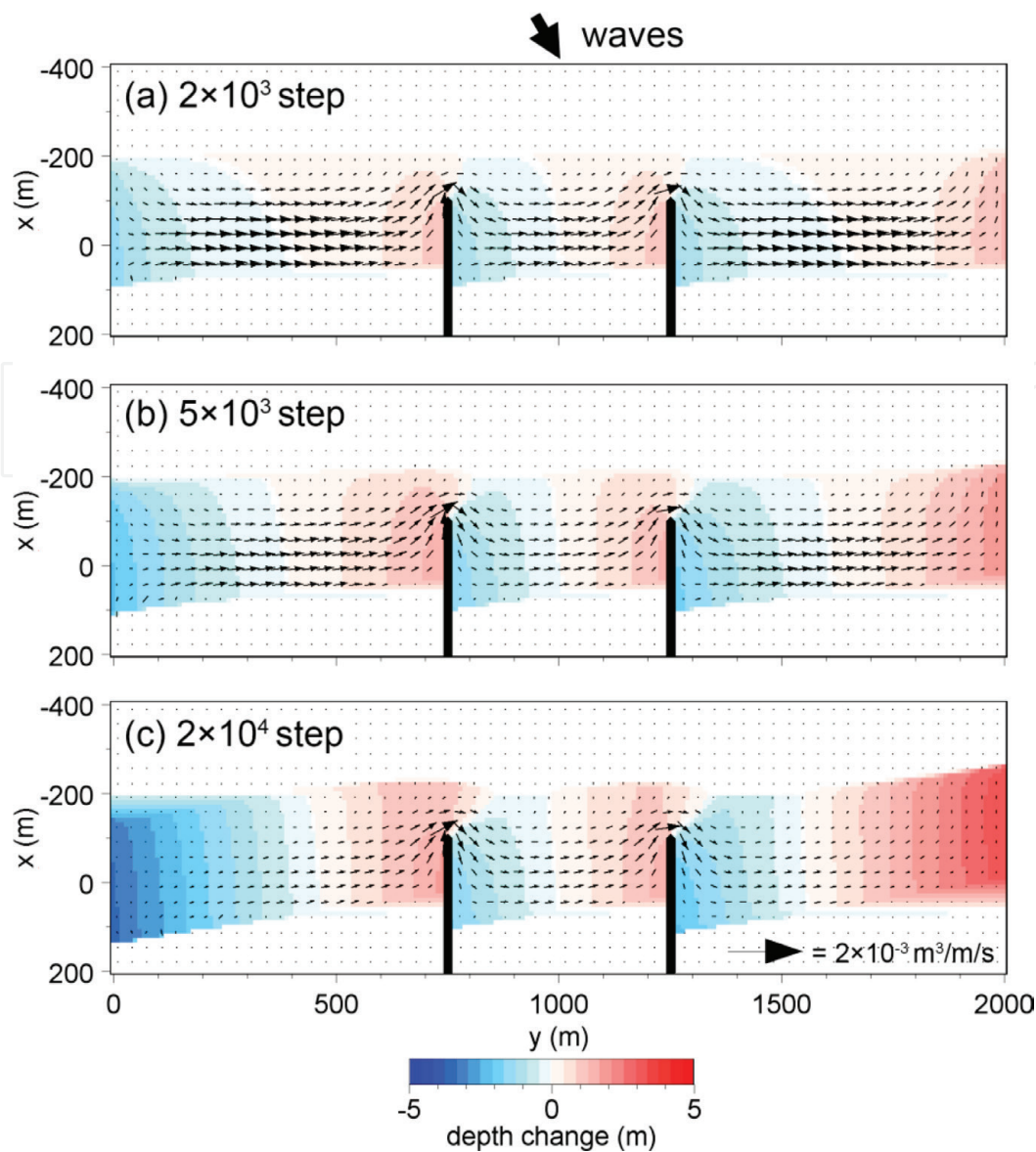
$$\tan\beta = (h_2 - h_1)/(a - b). \tag{2}$$

Figure 2.
Topographic changes and sand transport flux around two groynes installed on coast with parallel contours under oblique wave incidence.
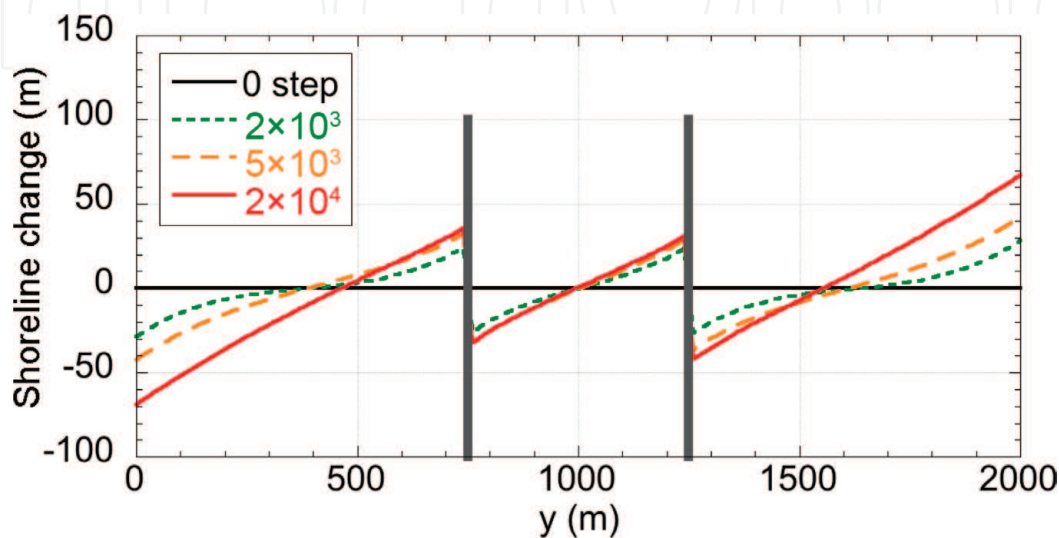
Figure 3.
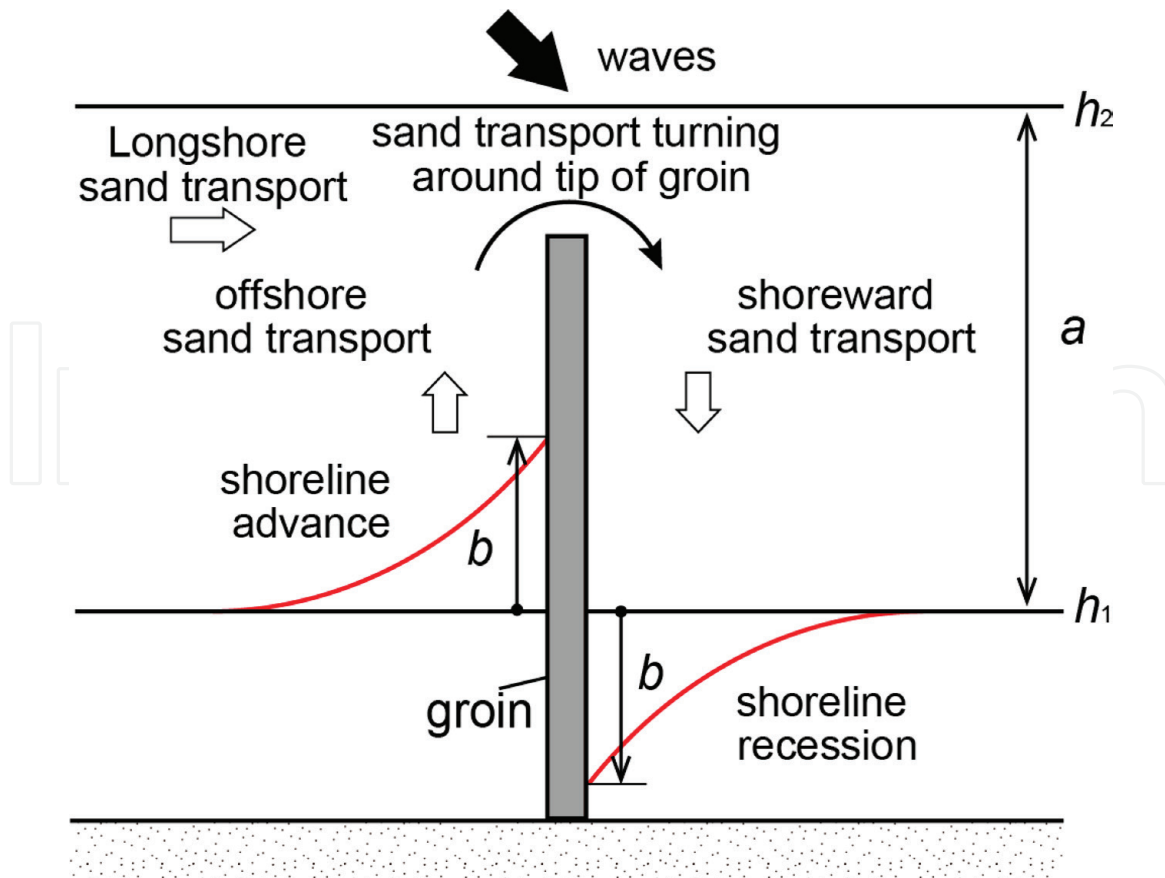*Shoreline changes around two groynes with time.*

Figure 4.
Schematic diagram of sand transport in vicinity of a groyne.

Eliminating h_1 and h_2 from Eqs. (1) and (2), we obtain Eq. (3).

$$\tan\beta \;=\; a/(a-b)\,\tan\beta_c. \tag{3}$$

In other words, the longitudinal slope increases greater than the equilibrium slope upcoast of the groyne, resulting in offshore sand transport. Similarly, the local seabed slope decreases downcoast of the groyne, as in Eq. (4), and shoreward sand transport arises, because the local slope becomes smaller than the equilibrium slope.

$$\tan\beta \;=\; a/(a+b)\,\tan\beta_c. \tag{4}$$

Thus, after the construction of the groyne, some specific contour line advances (retreats) upcoast (downcoast) because of the obstruction of longshore sand transport, causing the steeper (gentler) slope. This resulted in the offshore (shore-ward) sand transport, and sand transport turning around the tip of the groyne may take place (**Figure 4**). Because of the effects of the cross-shore and longshore sand transport offshore of the groyne, sand deposited near the shoreline upcoast is transported offshore near the tip of the groynes. The meandering of the contour lines offshore of the groynes corresponds to this motion of sand.

3. Beach changes around detached breakwaters

3.1 Calculation conditions

A calculation domain of 2000 m length and 600 m width in the longshore and cross-shore directions, respectively, was adopted, similarly to the groyne case. Assume that two permeable detached breakwaters of 250 m length and the wave transmission
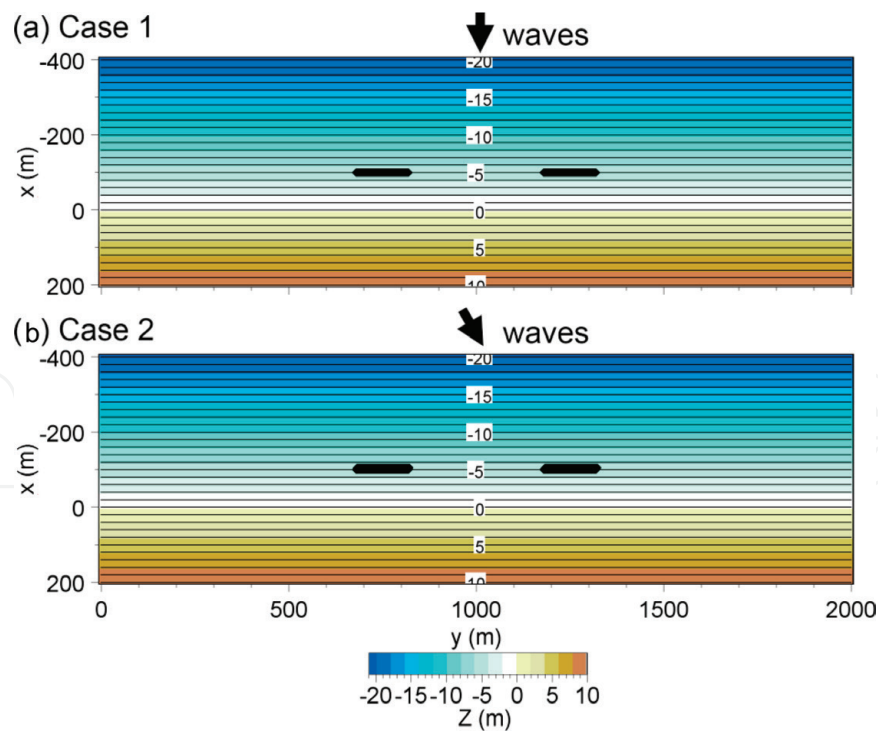
Figure 5.
Initial topography for calculating topographic changes around two detached breakwaters in Cases 1 and 2.

coefficient of K_t = 0.3 were placed 100 m offshore of the initial shoreline on a straight coast with parallel contours and the initial slope of 1/20. The interval of two detached breakwaters was set 350 m. As the incident wave direction, two directions were considered, i.e., waves were incident from the direction normal to the shoreline in Case 1, as shown in **Figure 5(a)** and obliquely incident relative to the normal to the initial shoreline at a breaker angle of 10° in Case 2, as shown in **Figure 5(b)**.

The wave-sheltering effect of the detached breakwaters was evaluated using the angular spreading method for irregular waves, given the directional spreading parameter S_{max} = 10 for wind waves [1], and the wave field was assumed to be constant over time. The berm height h_R and the depth of closure h_c were assumed to be 3 and 10 m, respectively, in both cases. The detached breakwaters were set at a depth of 5 m shallower than the depth of closure, so that part of littoral drift could pass through the area offshore of the detached breakwaters, when waves were obliquely incident relative to the normal to the shoreline. As the incident waves, waves with a breaker height of H_b = 3 m were assumed. The wave height was reduced on the lee of the detached breakwaters along with the change in wave direction because of the wave-sheltering effect of the detached breakwaters. These effects were evaluated by the angular spreading method for irregular waves [1], i.e., the wave energy flux was reduced by the multiplication of the square of the diffraction coefficient at each point, i.e., $(EC_g)_b' = K_d^2(EC_g)_b$, and the wave direction at each point was assumed to be the diffracted wave direction of θ_d ($\theta_w' = \theta_d$). In addition, $K_d H_b$ was employed for the wave height included in the Ozasa and Brampton's term [4]. The equilibrium slope was the same as the initial slope of $\tan\beta_c$ = 1/20. The other calculation conditions are summarized in **Table 2**.

3.2 Calculation results

3.2.1 Case 1

Figure 6 shows the wave field around detached breakwaters when waves were incident from the direction normal to the initial shoreline in Case 1. The symmetric wave-shelter zones were formed on the lee of the detached breakwaters. The wave-calm zone was formed near the shoreline, which may induce sand deposition behind the

Calculation methods	Angular spreading method for irregular waves [1] Type 2 BG model
Wave conditions	Incident waves: H_b = 3 m, wave direction θ_w = 0° and 10° in Cases 1 and 2, respectively, S_{max} = 10, $(EC_g)_b' = K_d^2 (EC_g)_b$, $\theta_w' = \theta_d$, $H_b' = K_d H_b$ for Ozasa and Brampton [4] term; K_d, diffraction coefficient; θ_d, diffracted wave direction
Berm height	h_R = 3 m
Depth of closure	h_c = 10 m
Equilibrium slope	$\tan\beta_c$ = 1/20
Depth distribution of sand transport	Cubic equation (Uda and Kawano [5])
Angle of repose slope	$\tan\beta_g$ = 1/2
Coefficients of sand transport	Coefficient of longshore sand transport K_x = 0.2 Coefficient of cross-shore sand transport K_y/K_x = 1.0 Coefficient of Ozasa and Brampton [4] term $K_2 = 1.62K_y$
Mesh size	$\Delta x = \Delta y$ = 10 m
Time intervals	Δt = 0.05 h
Duration of calculation	1.5×10^3 h (3×10^4 steps)
Boundary conditions	Shoreward and landward ends q_x = 0 Right and left boundaries q_y = 0
Other remarks	Wave transmission coefficient of detached breakwater: K_t = 0.3
Remarks	Lower minimum of 0.5 was set for $|\cos\alpha_b|$ in calculation of P value (Eq. (4) in Chap. 2) to avoid local discontinuity in topography

Table 2.
Calculation conditions.

detached breakwaters. **Figures 7** and **8** show the topographic changes and sand transport flux around two detached breakwaters in Case 1. Symmetric cuspate forelands were formed behind the detached breakwaters, and concave contours were formed in the opening of the detached breakwaters because of the formation of symmetric wave field. The response of the topographic changes behind the detached breakwaters was very quick, and the cuspate forelands were formed with time, as shown in **Figure 7(a)**,
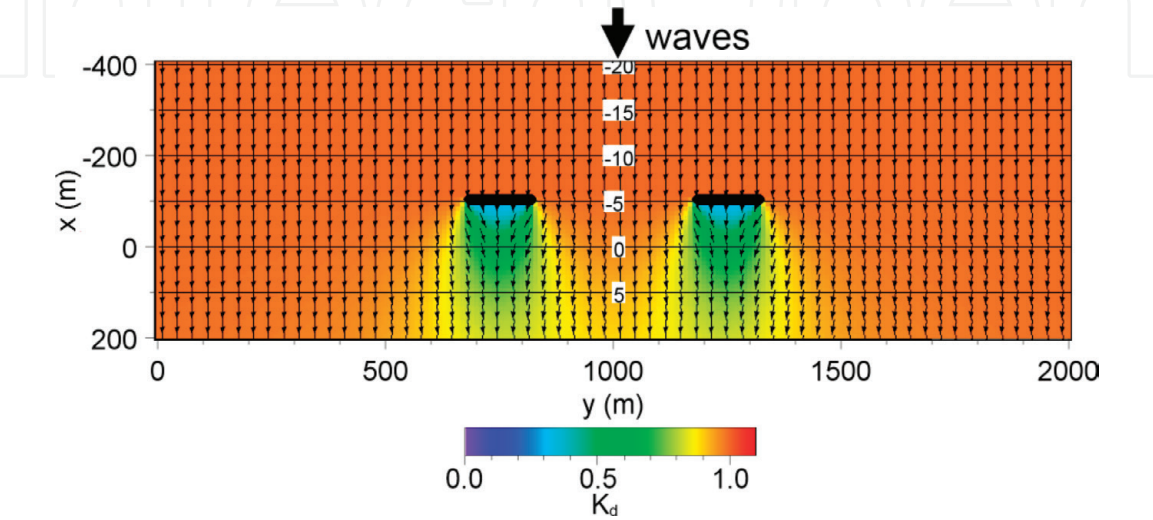

Figure 6.
Wave field around two detached breakwaters in Case 1 calculated using angular spreading method for irregular waves.
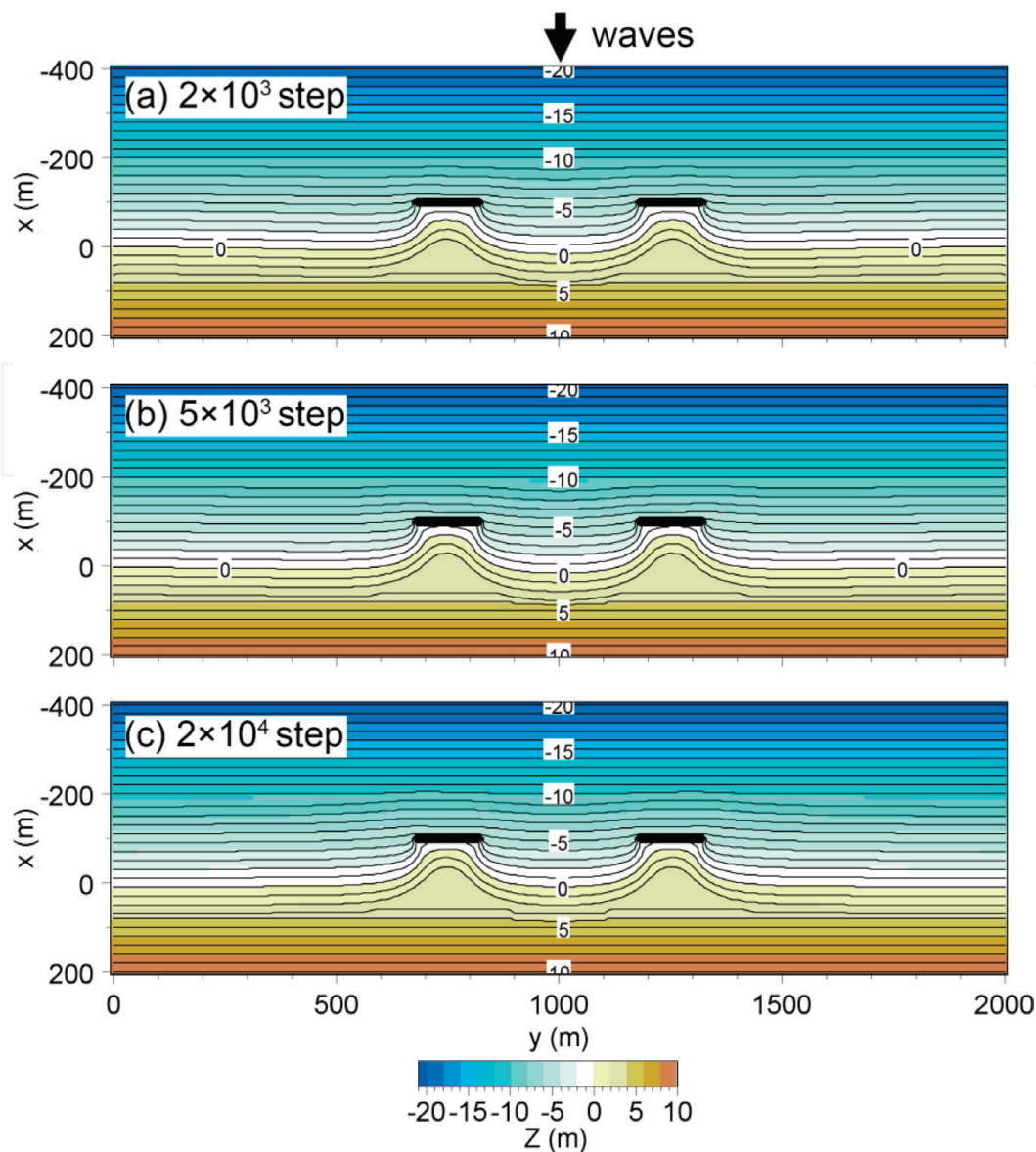
Figure 7.
Predicted topographies around two detached breakwaters in Case 1.

(b), and **(c)**. The sand transport flux decreased its intensity with the formation of cuspate forelands, as shown in **Figure 8(a)**, **(b)**, and **(c)**. **Figure 9** shows the shoreline changes around two detached breakwaters with time. The shoreline outside of the wave-shelter zone of the detached breakwaters receded, even though the amount of the shoreline recession was not so large, whereas the shoreline on the lee of the detached breakwaters markedly advanced because of the wave-sheltering effect of the detached breakwaters. It is concluded that the construction of detached breakwaters induces the concentrated accumulation of sand behind the detached breakwaters.

The response of the topographic changes behind the detached breakwaters was very quick, and the cuspate forelands were formed with time, as shown in **Figure 7(a)**, **(b)**, and **(c)**. The sand transport flux decreased its intensity with the formation of cuspate forelands, as shown in **Figure 8(a)**, **(b)**, and **(c)**.

3.2.2 Case 2

Similarly, **Figure 10** shows the wave field around detached breakwaters when waves were obliquely incident from the direction relative to the normal to the initial shoreline at a breaker angle of 10° in Case 2. Although the wave-shelter zones were also formed on the lee of the detached breakwaters, more wave energy was transported from the
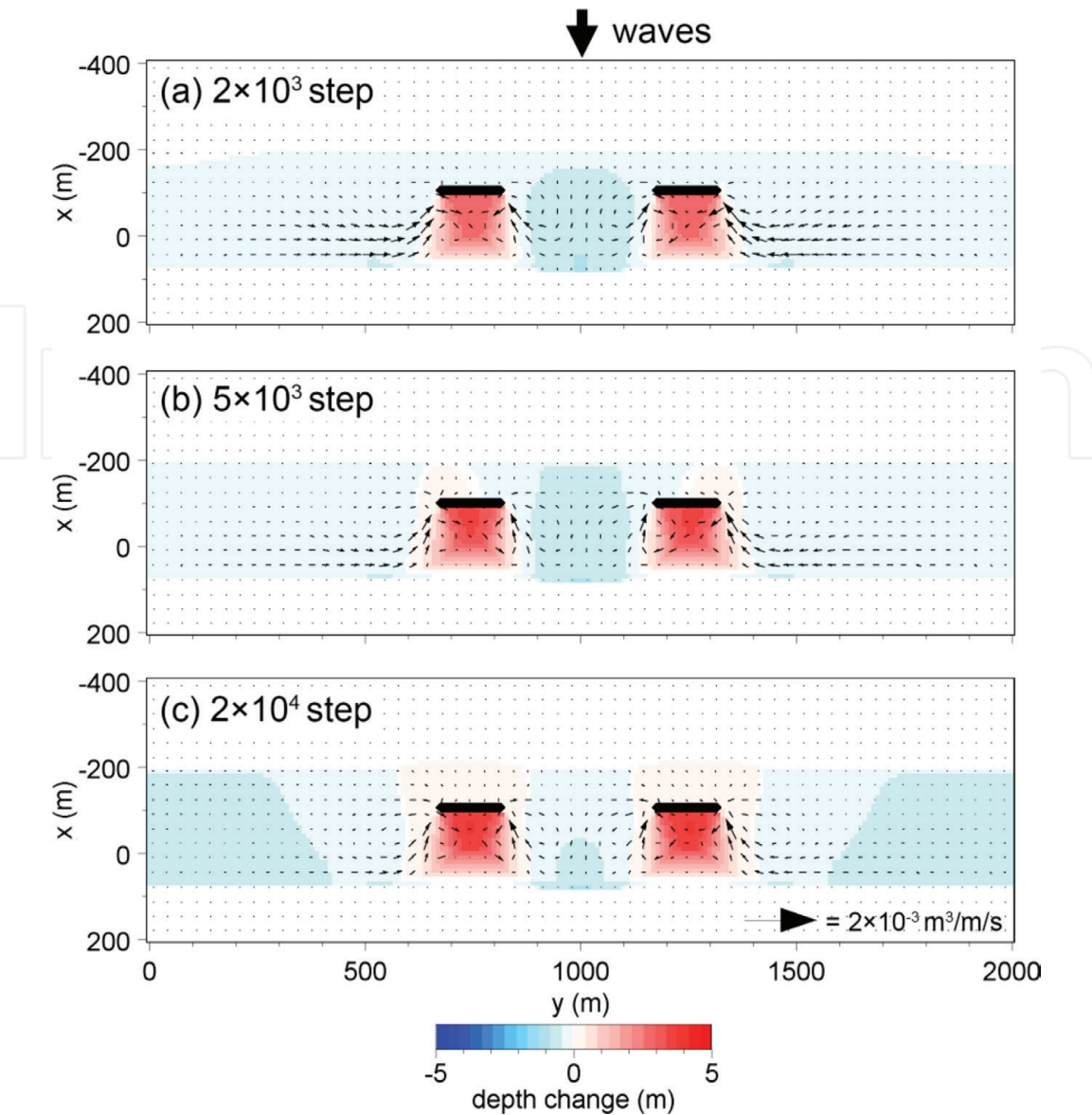
Figure 8.
Topographic changes and sand transport flux around two detached breakwaters in Case 1.
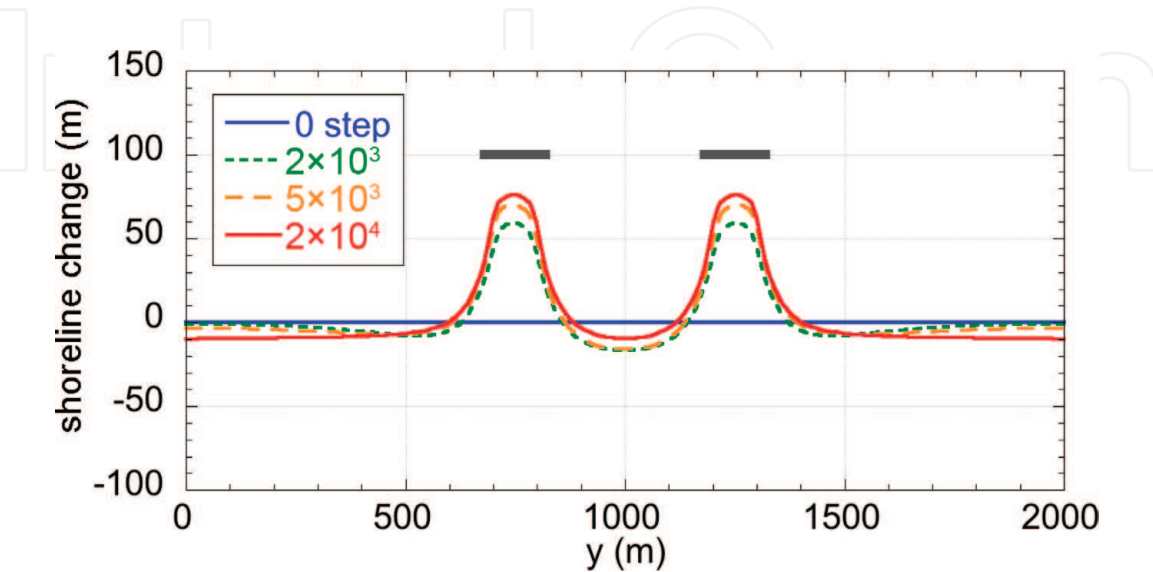
Figure 9.
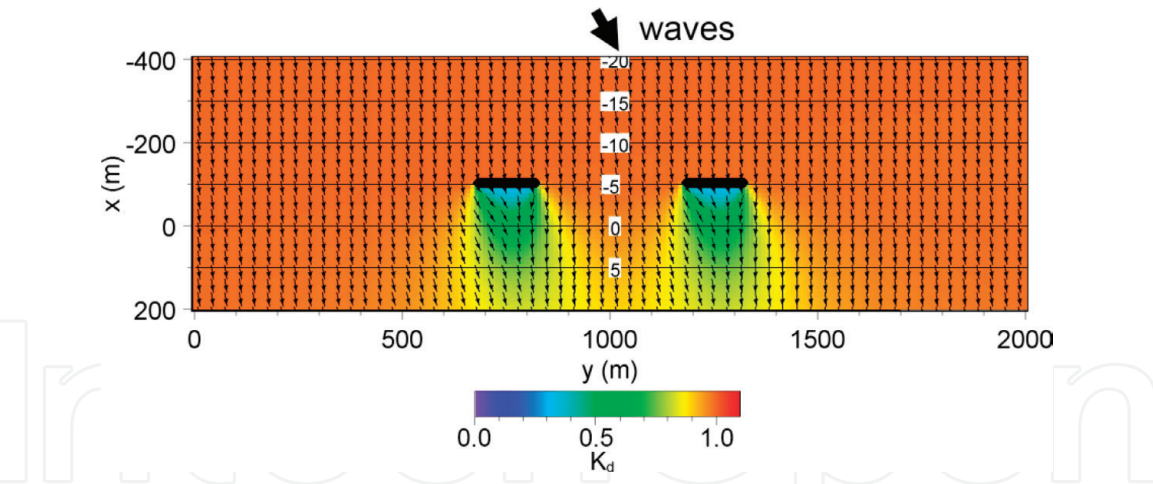*Shoreline changes around two detached breakwaters in Case 1.*

Figure 10.
Wave field around two detached breakwaters calculated using angular spreading method for irregular waves in Case 2.
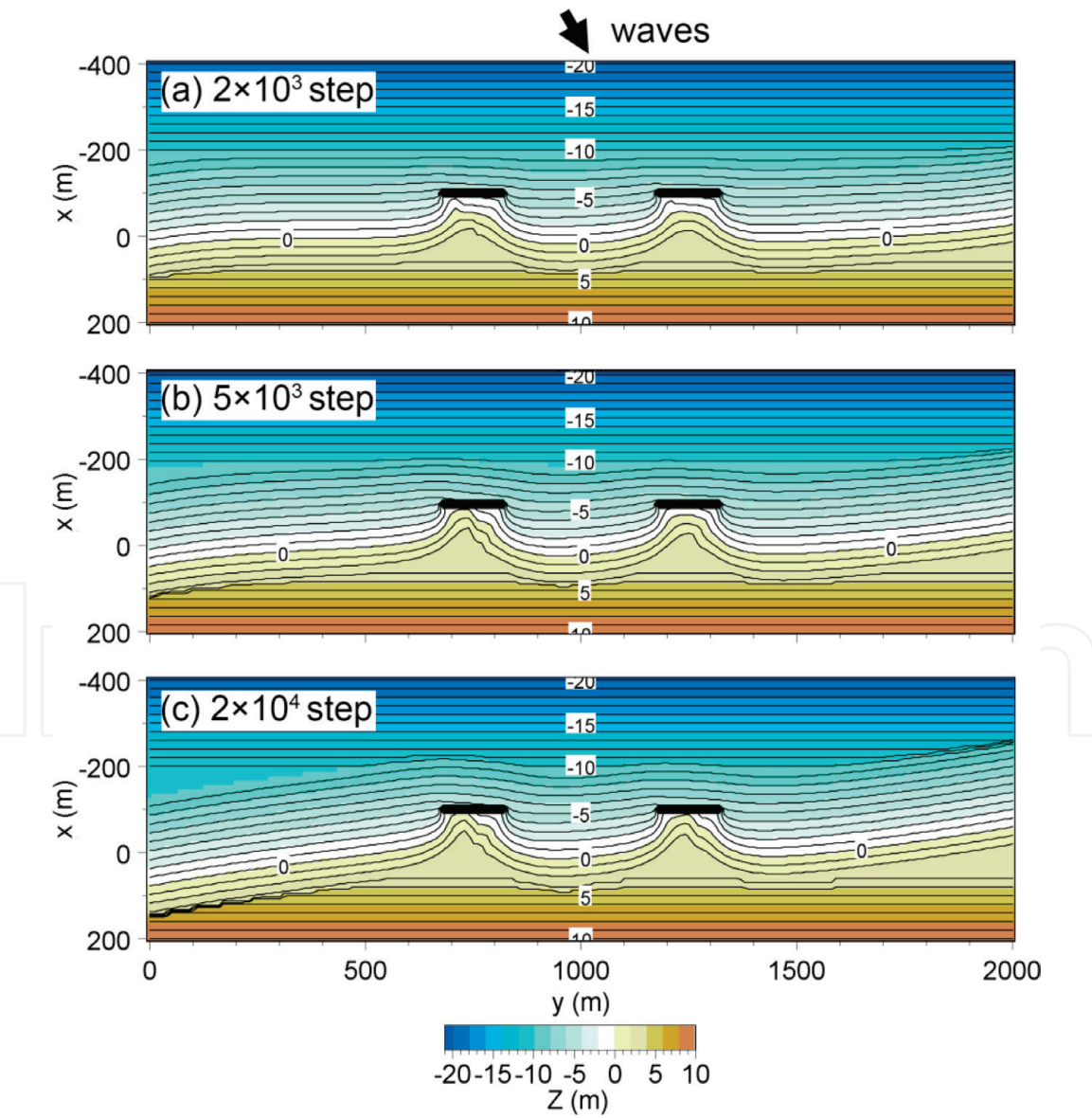

Figure 11.
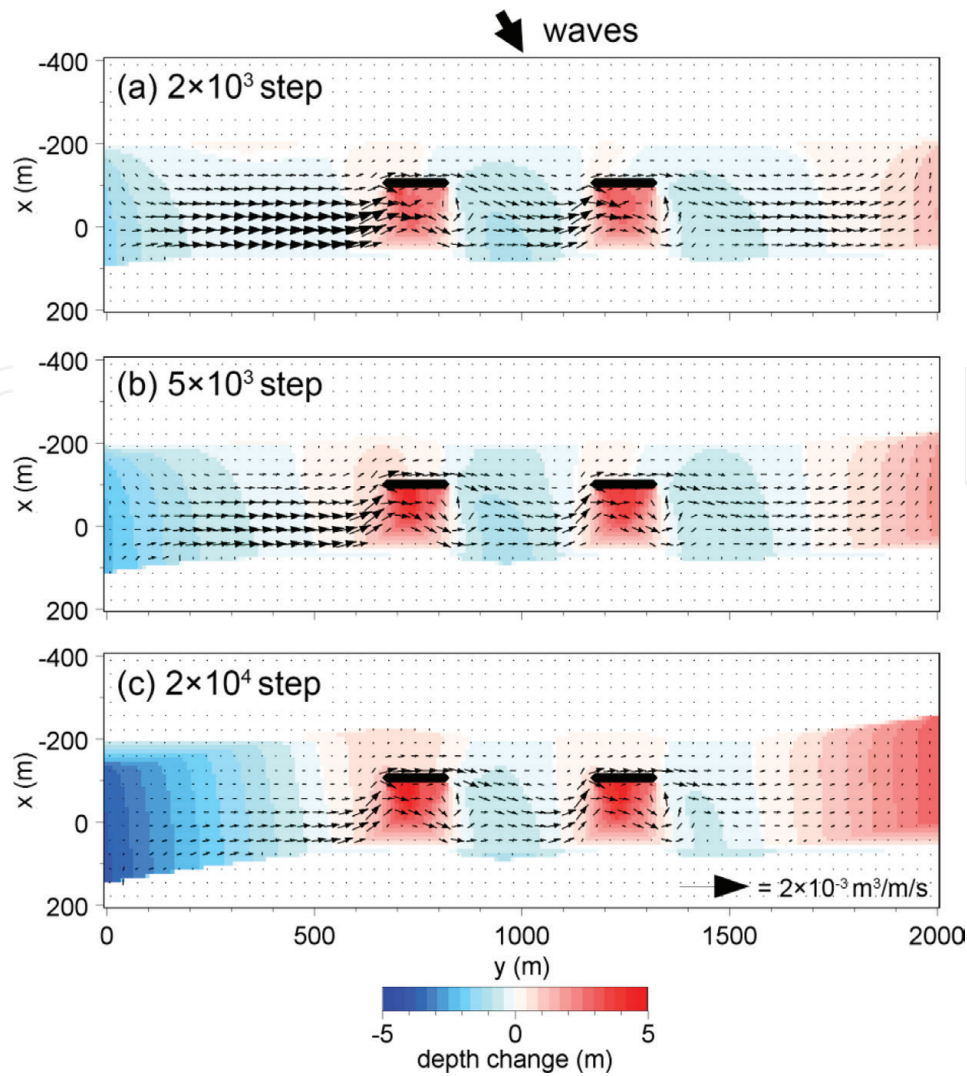*Predicted topographies around two detached breakwaters in Case 2.*

Figure 12.
Topographic changes and sand transport flux around two detached breakwaters in Case 2.

left on the lee of the detached breakwaters because of oblique wave incidence from the counterclockwise direction. The topographic changes and sand transport flux around two detached breakwaters in Case 2 are shown in **Figures 11** and **12**. Cuspate forelands were formed behind each detached breakwater after 2×10^3 steps, and concave contours were formed in the opening of the detached breakwaters (**Figure 11(a)**). Also, sand was transported rightward even offshore of the detached breakwaters (**Figure 12(a), (b),** and **(c)**), resulting in the meandering of contours offshore of the detached breakwaters,
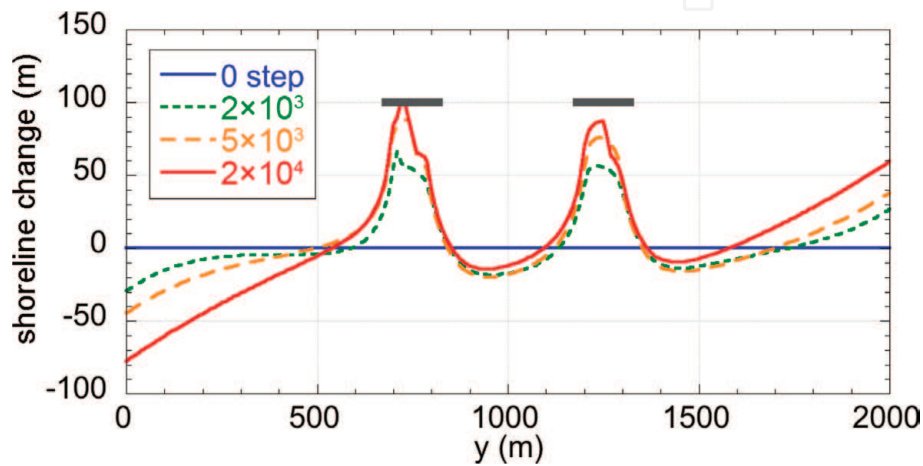
Figure 13.
Shoreline changes around two detached breakwaters in Case 2.

as shown in **Figures 11(b)** and **(c)**. **Figure 13** shows the shoreline changes around two detached breakwaters with time under oblique wave incidence. The shoreline upcoast of the detached breakwaters receded, whereas the shoreline downcoast of the detached breakwaters advanced because of the passage of part of longshore sand transport offshore of the detached breakwaters. Thus, it is concluded that sand is gradually transported downcoast by longshore sand transport under the condition that waves are obliquely incident to the direction normal to the shoreline, when permeable detached breakwaters were constructed on a coast.

4. Beach changes caused by offshore sand mining

4.1 Calculation conditions

Beach changes caused by sand mining offshore of a pocket beach was predicted using the Type 1 BG model. A calculation domain of 2000 m length and 600 m width in the longshore and cross-shore directions, respectively, was adopted,
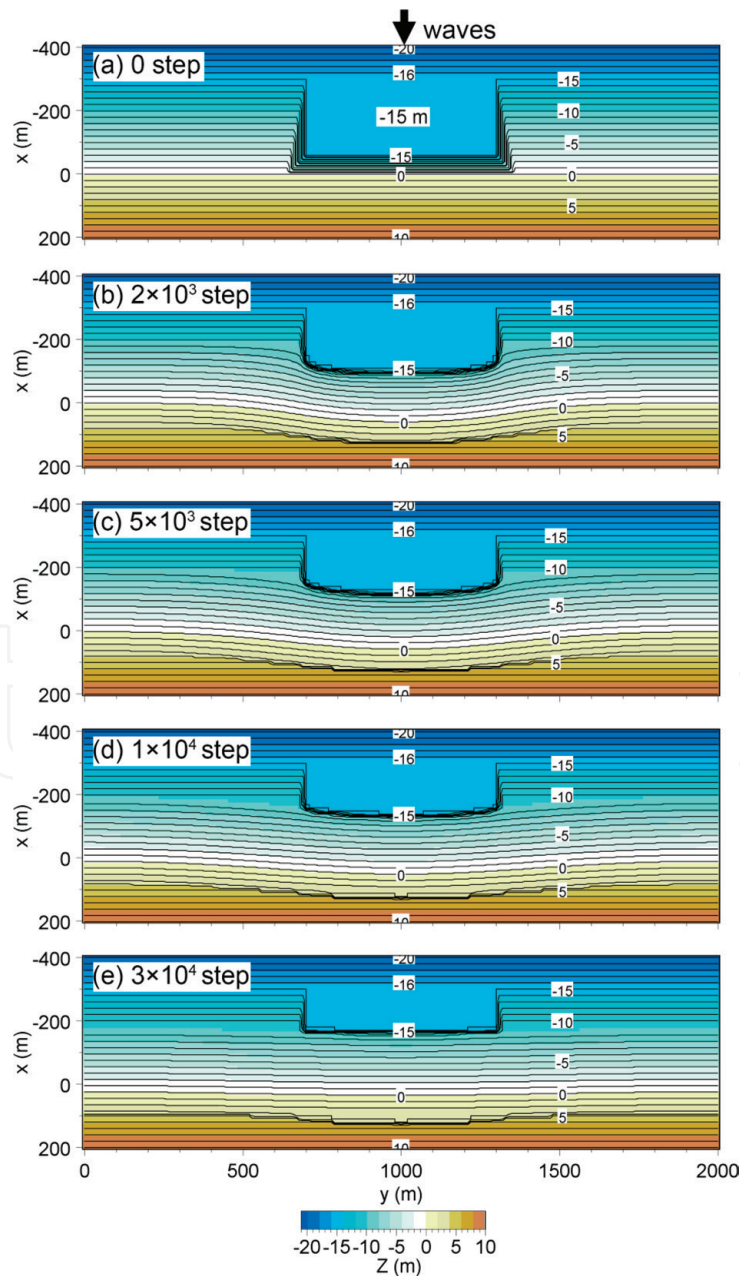

Figure 14.
Topographic changes around a hole excavated offshore of sandy beach with parallel contours.

similarly to the groyne case. Assume that the breaker height of H_b = 3 m and waves were assumed to be incident normal to the shoreline on a straight coast with a uniform seabed slope of 1/20. In the calculation, this constant breaker height was assumed anywhere in the calculation domain. Offshore mining was assumed to be carried out up to a depth of 15 m in a 600-m long and 300-m wide rectangular zone in the depth range between the shoreline and 15 m depth (**Figure 14(a)**). The excavated depth of the dredging hole at its center was large (reaching as deep as 15 m) relative to the original seabed, and h_R and h_c were assumed to be 3 and 10 m, respectively. The other calculation conditions are summarized in **Table 3**.

4.2 Calculation results

Figure 14 shows the refilling process of sand into the dredging hole under waves. The contour lines shallower than h_c of 10 m depth retreated around the dredging hole, and the dredging hole was gradually refilled over time because of the falling of sand through the landward steep slope. Sand refill began soon after dredging after 2×10^3 steps, and a concave shoreline was formed landward of the dredging hole, and a scarp began to be formed (**Figure 14(b)**). The dredging hole was further refilled due to wave action with time, as shown in **Figure 14(c)**. Since part of the sand on the sand dune was transported to the hole, the beach was severely eroded landward of the hole, resulting in the formation of a scarp of over 3 m height (**Figure 14(c)**). The size of the dredging hole decreased considerably as well as the longshore expansion of the eroded zone landward of the dredging hole after 10^4 steps (**Figure 14(d)**). Finally, the offshore dredging hole was refilled by 3×10^4 steps, and the remains of a dredging hole were left in the offshore zone together with the formation of a high scarp on the sand dune landward of the dredging hole (**Figure 14(e)**). It is concluded that a dredging hole is smoothed out with time in the region undergoing the dominant wave action, but a steep slope formed on the sand dune landward of the berm top has been left for a long time.

Calculation methods	Type 1 BG model
Wave conditions	Incident waves: H_b = 3 m, wave direction θ_w = 0°
Berm height	h_R = 3 m
Depth of closure	h_c = 10 m
Equilibrium slope	$\tan\beta_c$ = 1/20
Depth distribution of sand transport	Cubic equation (Uda and Kawano [5])
Angle of repose slope	$\tan\beta_g$ = 1/2
Coefficients of sand transport	Coefficient of longshore and cross-shore sand transport K_1 = 0.2 Coefficient of Ozasa and Brampton [4] term K_2 = 0.0
Mesh size	$\Delta x = \Delta y$ = 10 m
Time intervals	Δt = 0.05 h
Duration of calculation	1.5×10^3 h (3×10^4 steps)
Boundary conditions	Shoreward and landward ends, $q_x = 0$ Right and left boundaries, $q_y = 0$
Remarks	Lower minimum of 0.5 was set for $|\cos\alpha_b|$ in calculation of P value (Eq. (4) in Chap. 2) to avoid local discontinuity in topography

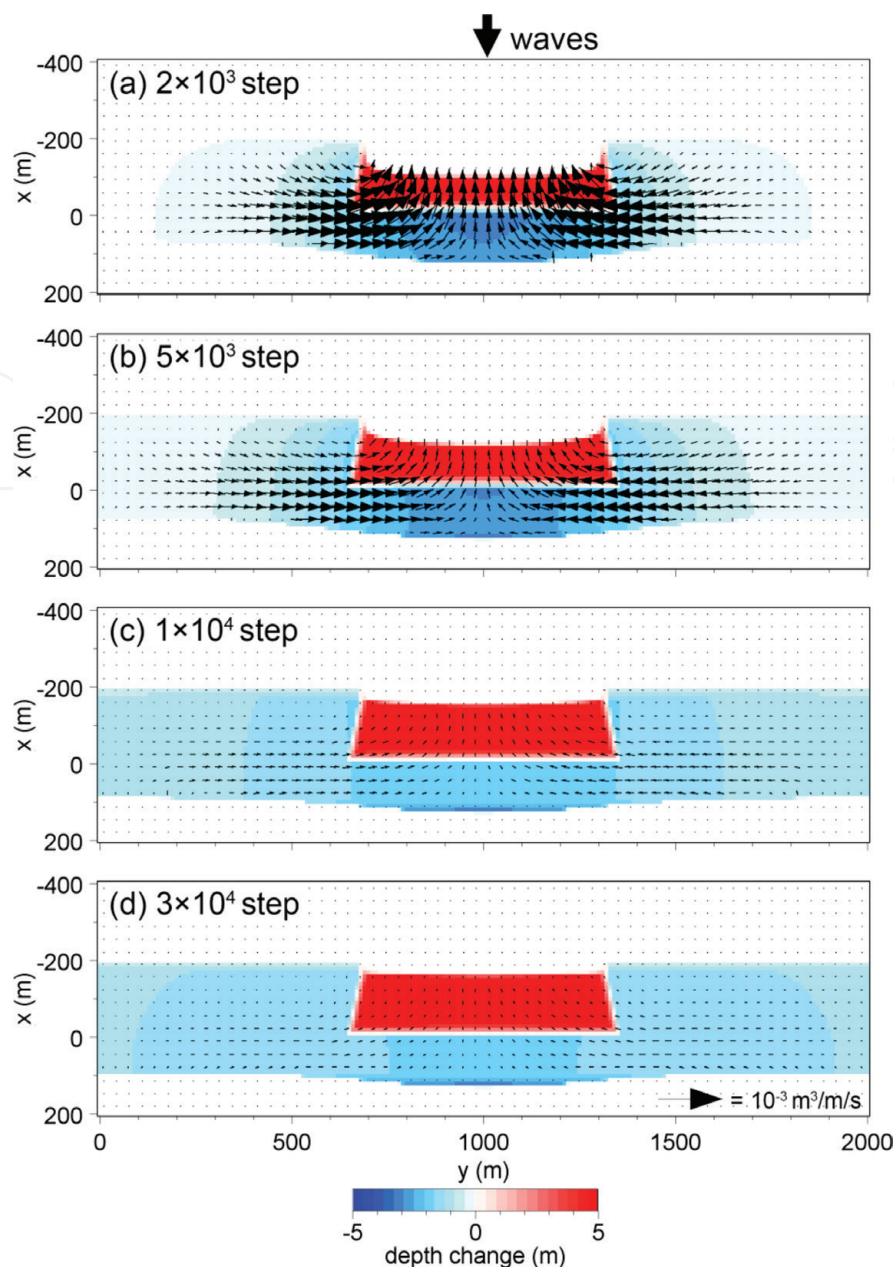**Table 3.**
Calculation conditions.

Figure 15.
Bathymetric changes and sand transport flux around a dredging hole excavated offshore of sandy beach with parallel contours.
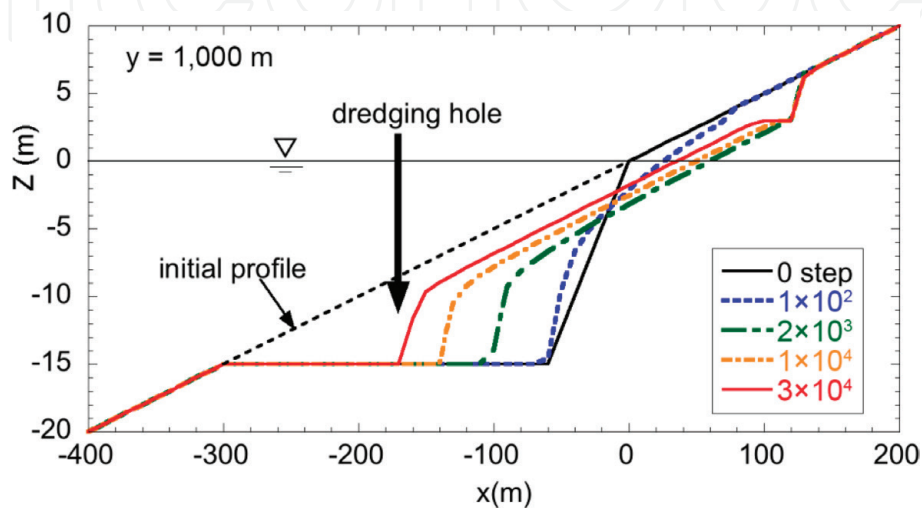

Figure 16.
Change in longitudinal profile with time along transect y = 1000 m.
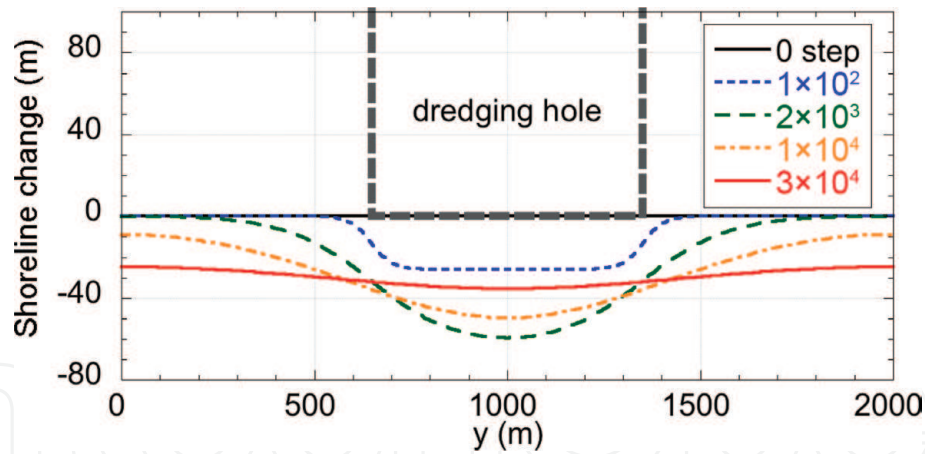
15

Figure 17.
Shoreline changes around a dredging hole with time.

The sand transport fluxes corresponding to the bathymetries at each step shown in **Figure 14** are shown in **Figure 15**. At the initial stage, strong fluxes toward the dredging hole from the nearby area were generated (**Figure 15(a)**), and these fluxes ceased with time as the dredging hole was refilled, as shown in **Figures 15(b)**, **(c)**, and **(d)**. The topographic changes can be realized from the change in longitudinal profile through the center line of the hole (**Figure 16**). At the initial stage, the landward slope of the dredging hole was so steep that sand was refilled from the shoreward slope, forming a steep slope with angle of repose of sand in the zone deeper than the depth of closure.

The shoreline changes around a dredging hole with time can be drawn as in **Figure 17**. After 100 steps, the shoreline immediately behind the offshore dredging hole retreated. With time, the shoreline recession zone expanded alongshore. Note that the offshore sand mining in a zone shallower than h_c affects the beach in the entire zone together with the formation of a high scarp on the sand dune.

5. Beach changes associated with extension of oblique port breakwater

5.1 Calculation conditions

A calculation domain of 2000 m length and 600 m width in the longshore and cross-shore directions, respectively, was adopted to predict beach changes associated with the extension of an oblique breakwater on a coast with parallel contours. **Figure 18**
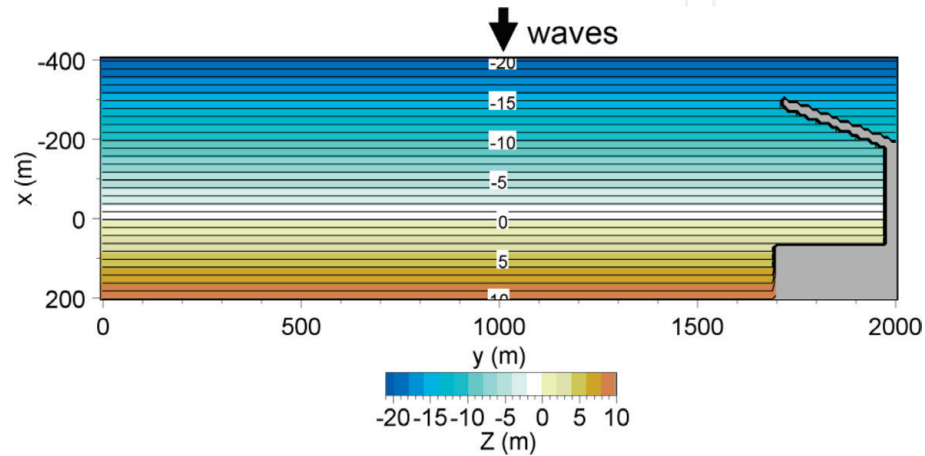

Figure 18.
Initial topography of coast with parallel contours and setup of an oblique breakwater.

16

Calculation methods	Type 2 BG model Angular spreading method for irregular waves [1]
Wave conditions	Incident waves: H_b = 3 m, wave direction θ_w = 0°, S_{max} = 10, $(EC_g)_b' = K_d^2 (EC_g)_b$, $\theta_w' = \theta_d$, $H_b' = K_d H_b$ for Ozasa and Brampton [4] term; K_d, diffraction coefficient; θ_d, diffracted wave direction
Berm height	$h_R' = K_d h_R$ (h_R = 3 m), K_d: diffraction coefficient
Depth of closure	$h_c' = K_d h_c$ (h_c = 10 m), K_d: diffraction coefficient
Equilibrium slope	$\tan\beta_c = 1/20$
Depth distribution of sand transport	Cubic equation (Uda and Kawano [5])
Angle of repose slope	$\tan\beta_g = 1/2$
Coefficients of sand transport	Coefficient of longshore sand transport K_x = 0.2 Coefficient of cross-shore sand transport K_y/K_x = 1.0 Coefficient of Ozasa and Brampton [4] term $K_2 = 1.62K_y$
Mesh size	$\Delta x = \Delta y = 10$ m
Time intervals	$\Delta t = 0.05$ h
Duration of calculation	10×10^3 h (5×10^4 steps)
Boundary conditions	Shoreward and landward ends q_x = 0 Right and left boundaries q_y = 0
Remarks	Lower minimum of 0.5 was set for $|\cos\alpha_b|$ in calculation of P value (Eq. (4) in Chap. 2) to avoid local discontinuity in topography

Table 4.
Calculation conditions.

shows the initial topography of the coast and the setup of an oblique breakwater, which was constructed at the right corner of the calculation domain. The wave field which was affected by the extension of the breakwater was determined by the angular spreading method for irregular waves [1], assuming that waves with the breaker height of H_b = 3 m were incident normal to the shoreline on a straight coast with a uniform seabed slope of 1/20. The wave field was assumed to be constant over time. The wave-sheltering effect of an oblique breakwater was evaluated similarly to the method in the case of the detached breakwater, as described in Section 3.

In the calculation of beach changes, h_R and h_c were assumed to be 3 and 10 m, respectively, in the zone without the wave-sheltering effect far from the oblique
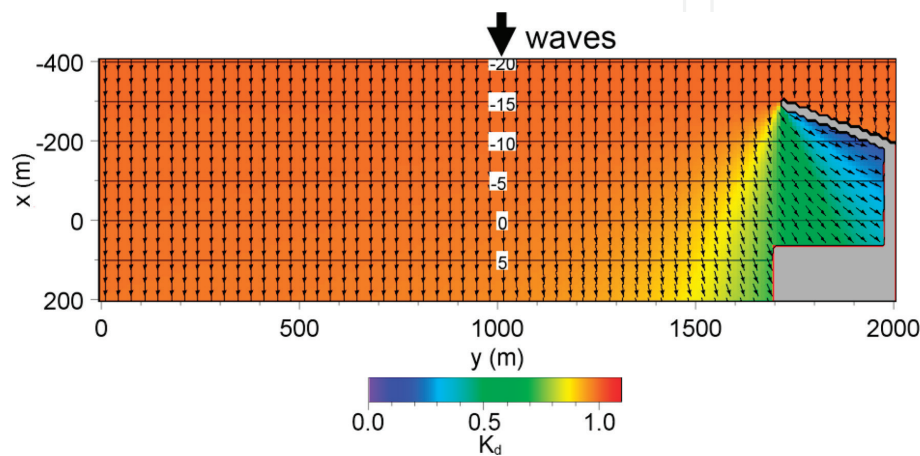

Figure 19.
Wave field around an oblique breakwater.

breakwater. In the wave-shelter zone, the berm height $h_R{'}$ was estimated from h_R multiplied by the diffraction coefficient K_d ($h_R{'} = K_d h_R$). Similarly, the depth of closure $h_c{'}$ was estimated from h_c multiplied by the diffraction coefficient K_d ($h_c{'} = K_d h_c$). The equilibrium slope was set 1/20. The calculation conditions are summarized in **Table 4**.

5.2 Calculation results

Figure 19 shows the wave field around an oblique breakwater. Owing to the wave-diffraction effect of the oblique breakwater, the wave-shelter zone expanded to the lee of the breakwater. The longshore change in wave height owing to the wave-sheltering effect of the breakwater caused rightward longshore current
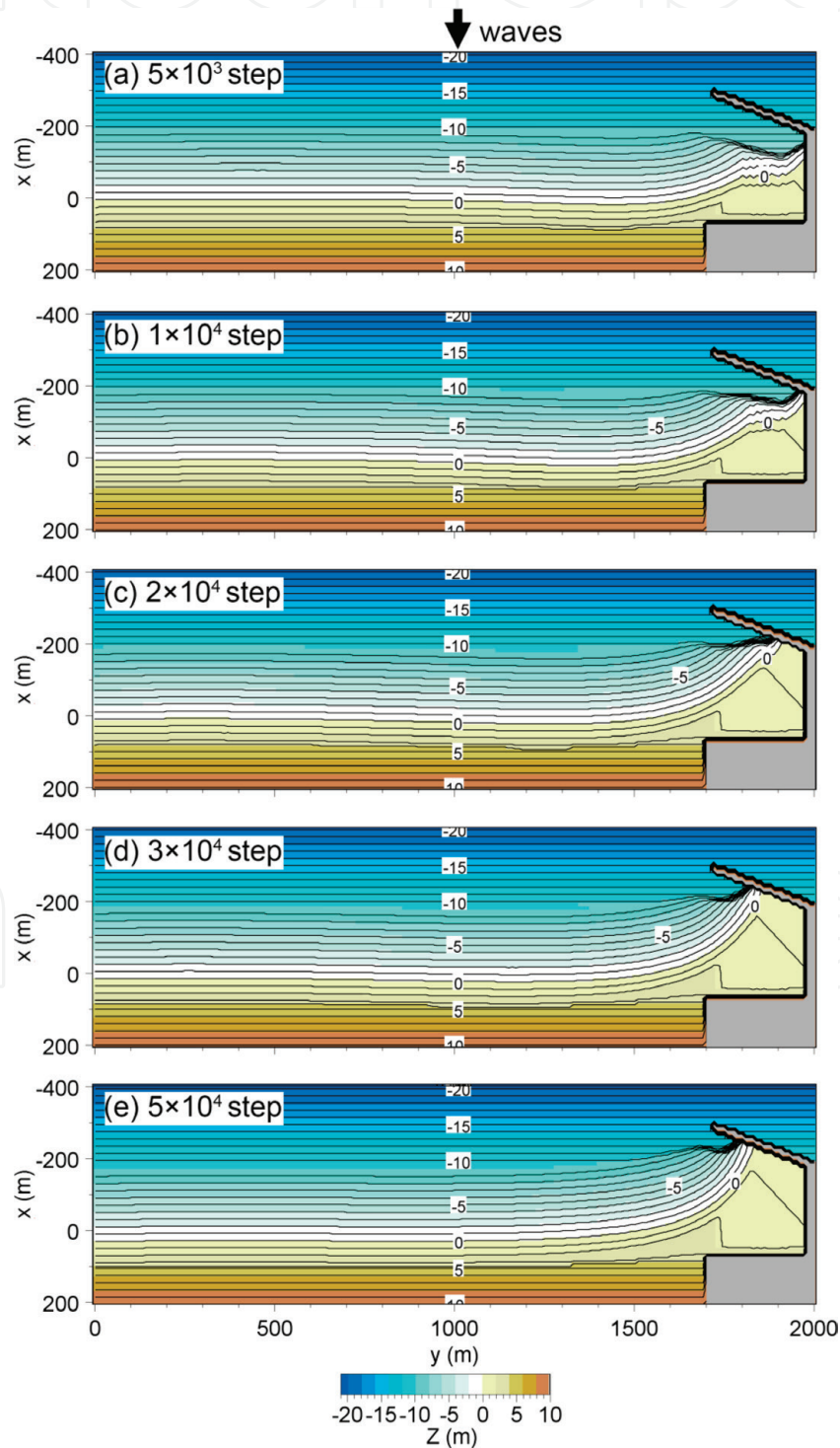
Figure 20.
Successive deposition of sand inside the wave-shelter zone produced by extension of a long port breakwater.

(longshore sand transport), resulting in erosion outside the wave-shelter zone and sand deposition inside the wave-shelter zone. **Figure 20** shows the topographic changes around an oblique breakwater at each step. Owing to the occurrence of longshore sand transport from outside to inside the wave-shelter zone, sand was deposited on the lee of the breakwater after 5×10^3 steps, and sand fell down into the deep area immediately landward of the breakwater while forming a steep slope of angle of slope of sand (**Figure 20(a)**). In contrast, beach erosion far from the breakwater was gradual. With time, sand deposition behind the oblique breakwater continued, and a large amount of sand was deposited inside the port with filling
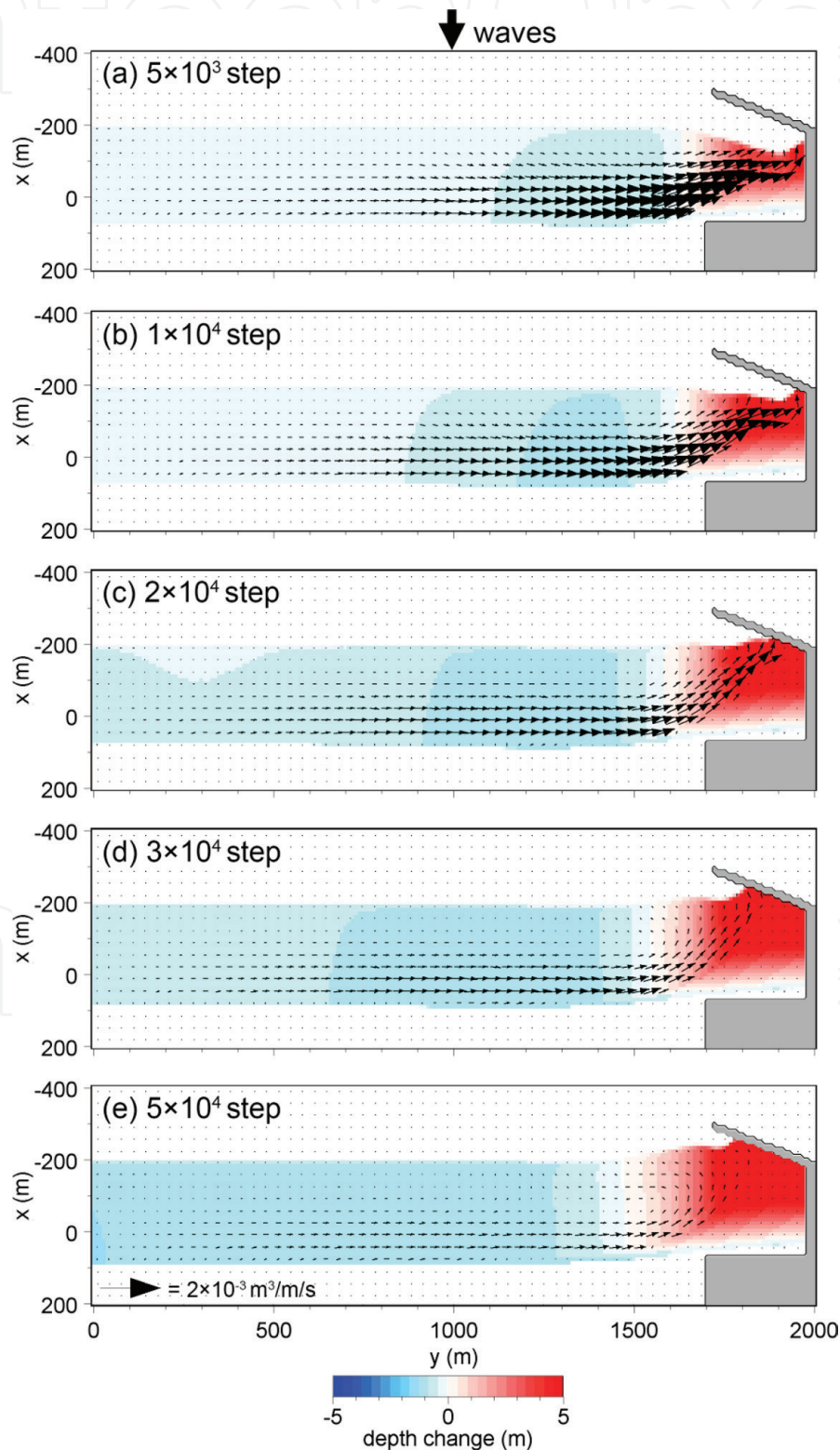
Figure 21.
Topographic changes and sand transport flux around an oblique breakwater.

up of the whole area up to 5×10^4 steps, as in the successive changes in topography shown in **Figure 20**.

As regards the sand transport flux at each stage, strong rightward longshore sand transport was induced in the area shoreward of the tip of the oblique breakwater, and the sand transport flux diminished with the sand accumulation inside the wave-shelter zone, as shown by the successive changes in sand transport flux in the vicinity of the port breakwater in **Figure 21**. In reality, such sand deposited on the lee of the wave-shelter zone of the breakwater would have been removed in general to maintain the navigation channel. In such a case, the shoreline recession outside the wave-shelter zone significantly increases, because total amount of sand on the nearby coast decreases by repeated removal of sand.

The shoreline recession and advance outside and inside the wave-shelter zone of an oblique breakwater are shown in **Figure 22**. A large amount of sand was deposited in the wave-shelter zone, resulting in a large shoreline advance, whereas outside the wave-shelter zone, the shoreline recession was much smaller than that inside the wave-shelter zone.
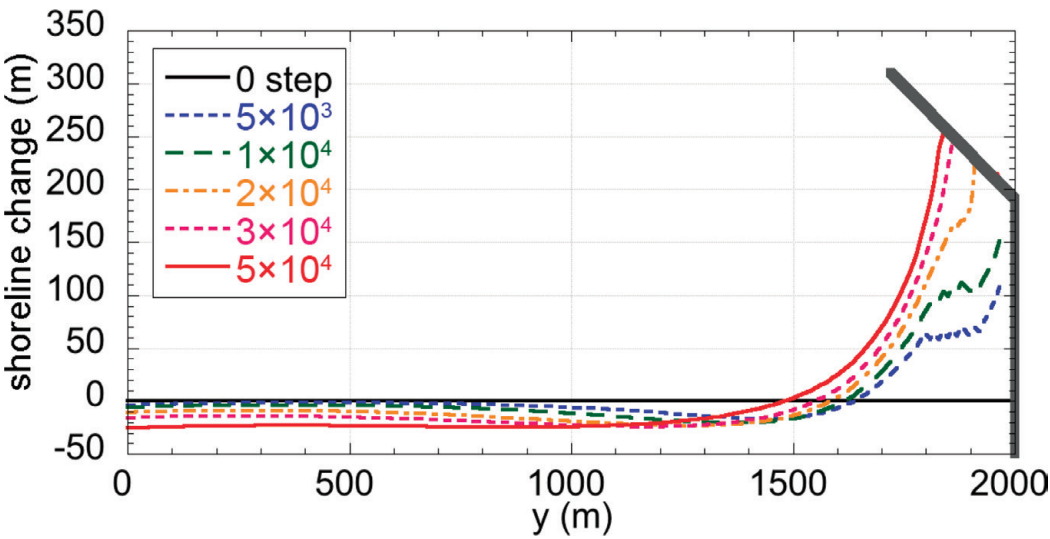

Figure 22.
Shoreline recession and advance outside and inside wave-shelter zone, respectively, formed by an oblique breakwater.
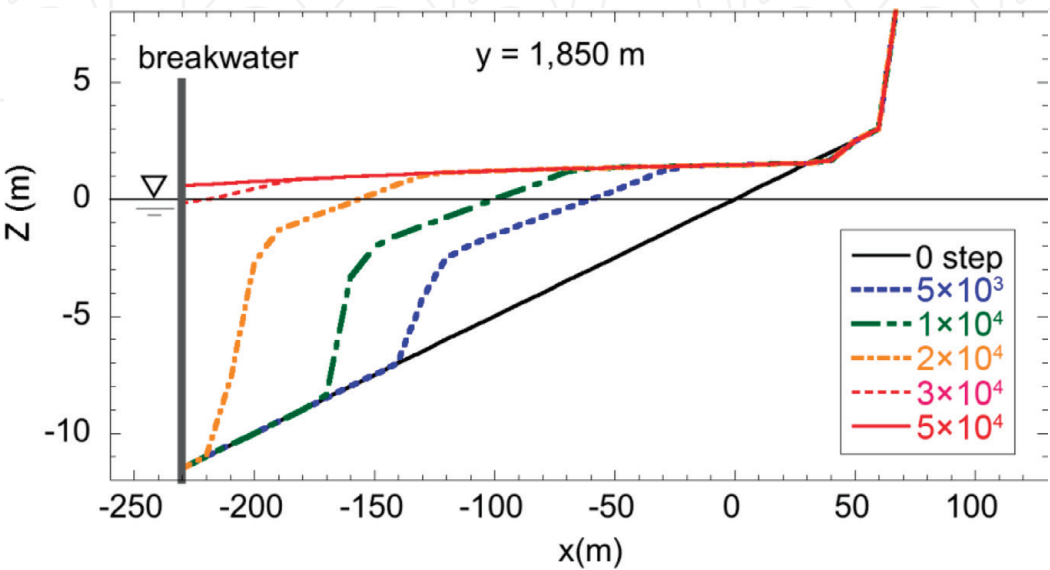

Figure 23.
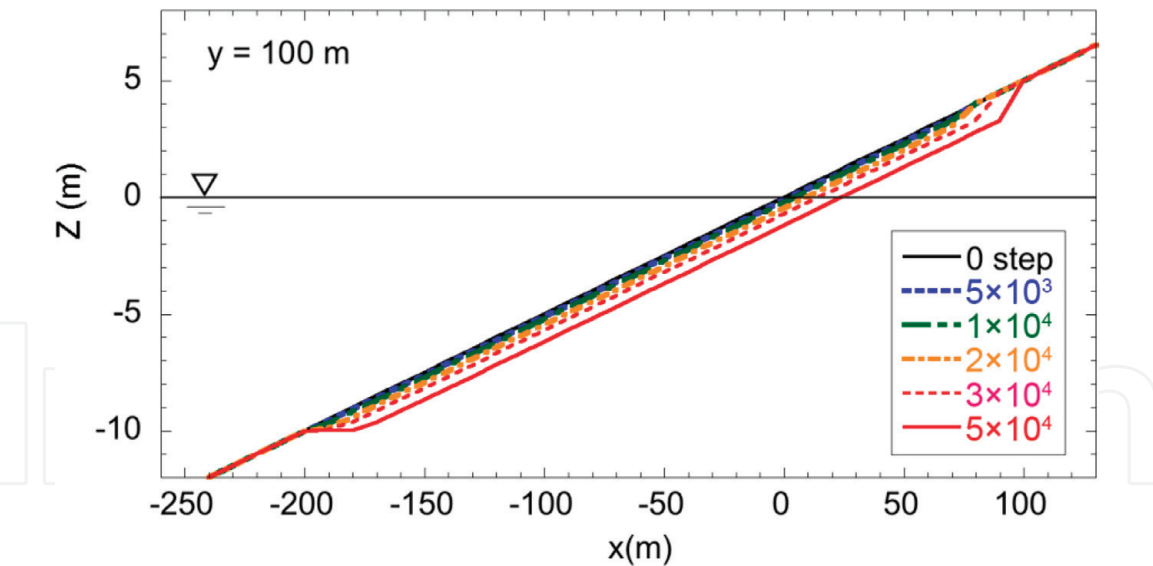*Change in longitudinal profile along transect y = 1850 m.*

Figure 24.
Change in longitudinal profile along transect y = 100 m.

Figures 23 and **24** show the change in longitudinal profiles along transects *y* = 1850 m in the accumulation area and *y* = 100 m in the eroded area outside the wave-shelter zone. A large amount of sand was deposited immediately behind the breakwater with the formation of steep slope of the angle of slope. In contrast, far from the wave-shelter zone, the longitudinal profile retreated parallelly, and a scarp was formed on the backshore.

6. Sand deposition inside a port surrounded by an oblique breakwater and a jetty

6.1 Calculation conditions

A calculation domain of 2000 m length and 600 m width in the longshore and cross-shore directions, respectively, was adopted, similarly to that in the former cases. **Figure 25** shows the initial topography of the coast and the setup of an oblique breakwater, which was constructed at the right corner of the calculation
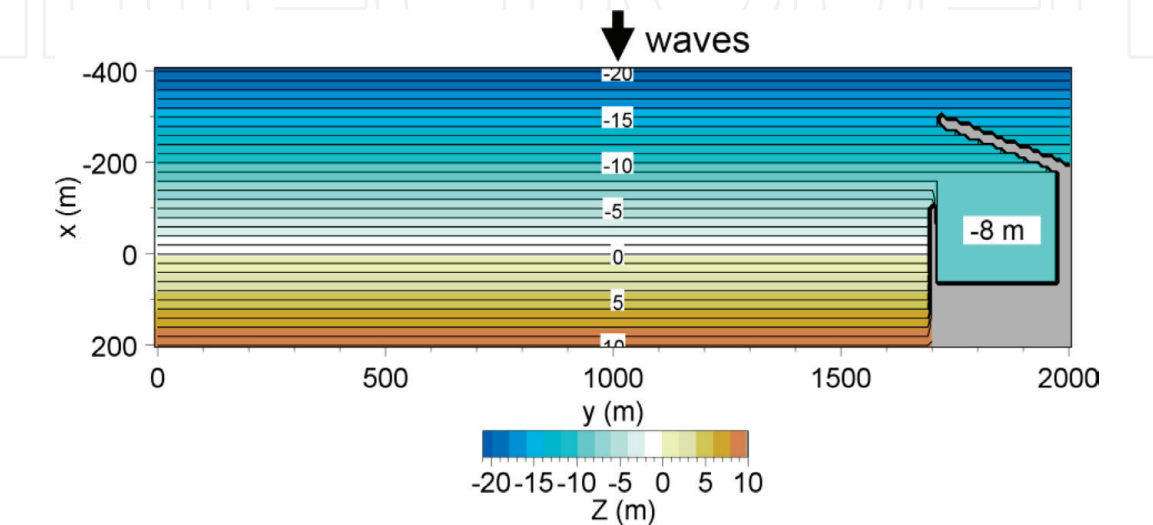

Figure 25.
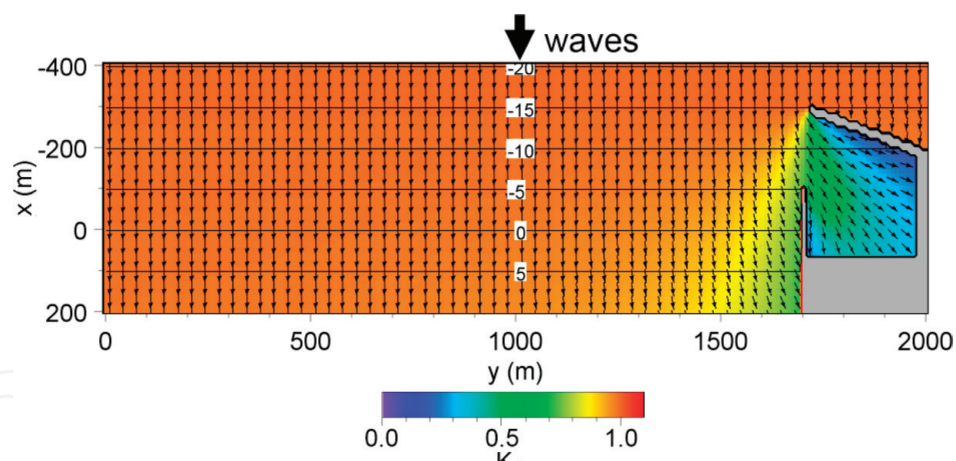*Initial topography of coast and setup of oblique breakwater and jetty.*

Figure 26.
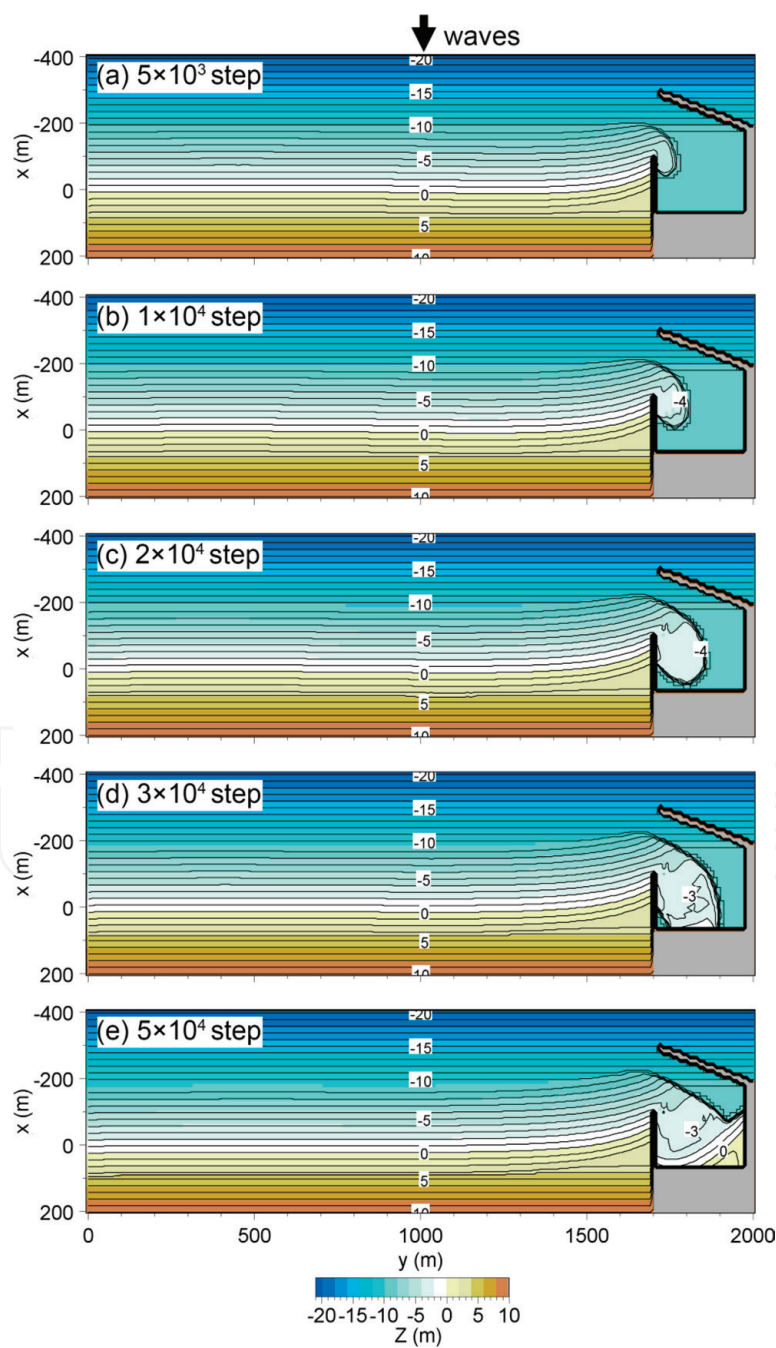*Wave field around port breakwater and a jetty.*

Figure 27.
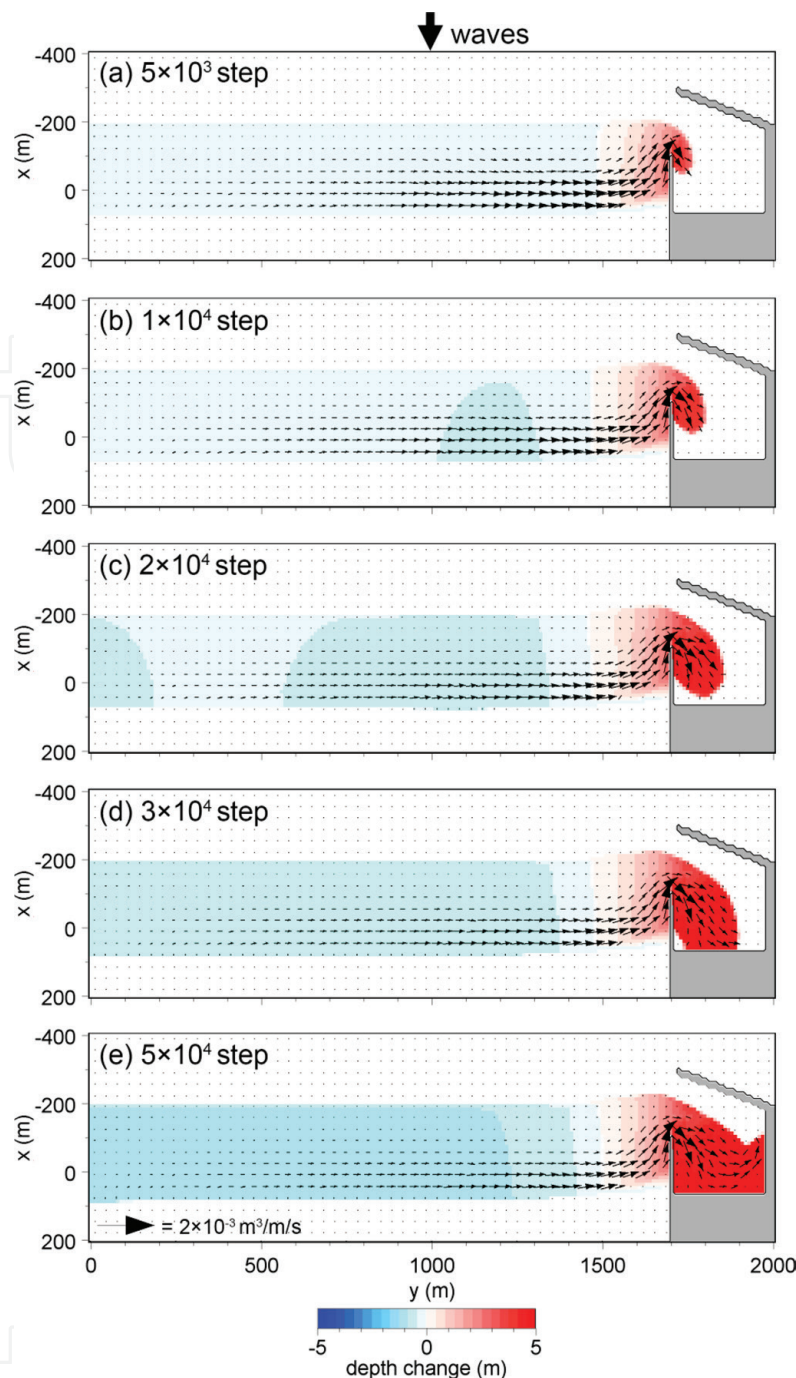*Successive beach changes inside port and erosion on the nearby coast.*

Figure 28.
*Sand transport flux corresponding to beach changes shown in **Figure 27**.*

domain, together with a jetty with a point depth of 5 m to prevent sand from depositing inside the port. At the initial stage, the depth of the port is maintained as a constant depth of 8 m, and an impermeable jetty separates the sandy beach of a slope of 1/20 and the port area. The wave field which will be affected by the extension of the breakwater was determined similarly by the angular spreading method for irregular waves [1], assuming that waves with a breaker height of H_b = 3 m were incident normal to the shoreline on a straight coast. The wave-sheltering effect of an oblique breakwater was evaluated similarly to the method in the case of the detached breakwater, as described in Section 3. In the calculation of beach changes, h_R and h_c were assumed to be 3 and 10 m, respectively, in the zone without the wave-sheltering effect far from the oblique breakwater. In the wave-shelter zone, the berm height h_R' and the depth of closure h_c' were calculated by the same method described in Section 5 ($h_R' = K_d h_R$ and $h_c' = K_d h_c$).

Figure 26 shows the wave field around the port with a jetty at the mouth of the port. Because of the wave-sheltering effect of the breakwater, longshore sand transport toward the wave-shelter zone was induced. The calculation conditions in this case are the same as in Section 5 (**Table 4**).

6.2 Calculation results

Figure 27 shows the successive beach changes inside the port and erosion on the nearby coast. Rightward longshore sand transport took place because of the wave-sheltering effect of the oblique breakwater, and such sand transport turned around the tip of the jetty, causing the sand deposition immediately right of the jetty. Gradual deposition of sand inside the port was well predicted, as shown in **Figure 27(a)-(e)**. The shape of the sand deposition area was similar to a sand spit with a flat top and steep slope around the sand deposition area. **Figure 28** shows the sand transport flux corresponding to the beach changes shown in **Figure 27** at each step. Strong sand transport occurred around the tip of the impermeable jetty, and such
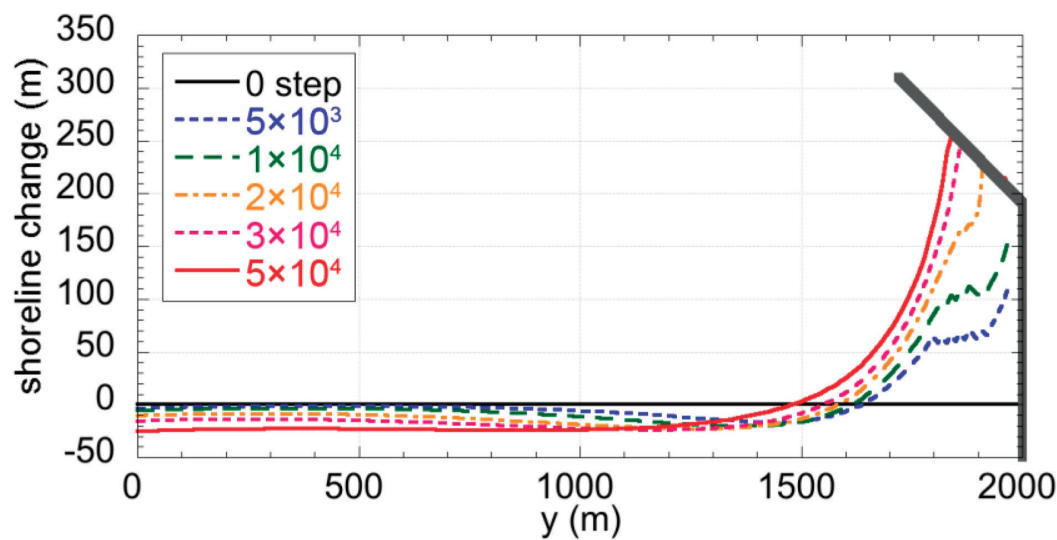

Figure 29.
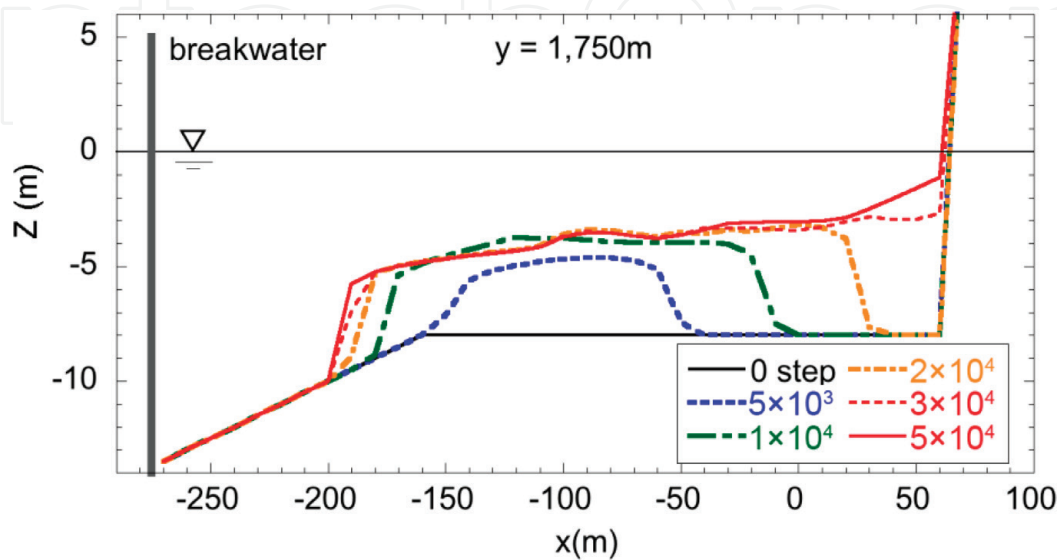*Shoreline changes around port.*

Figure 30.
Changes in longitudinal profiles along transect y = 1750 m.

sand transport flux continued for a long time, regardless of the time steps, as shown in **Figures 28(a)-(e)**. Finally, erosion occurred over a widespread area even in the area far from the offshore breakwater, whereas a large amount of sand accumulated behind the breakwater.

The shoreline changes around the port can be drawn as in **Figure 29**. The shoreline recession continued with time, even though accretion area did not increase. This is because a large amount of sand was deposited in the port area with a large water depth. Finally, the changes in longitudinal profiles along transect y = 1750 m across the sand deposition area and transect y = 100 m across the erosion zone are shown in **Figures 30** and **31**, respectively. Along transect y = 1750 m, sand deposition zone with a flat depth of approximately 3 m expanded over time. In contrast, in the erosion zone, longitudinal profiles retreated parallel each other.

The effect of a jetty extended at the entrance of the port in preventing sand from depositing inside the port can be evaluated in terms of the volume of sand deposited inside the port with/without a jetty. **Figure 32** shows the change in sand volume
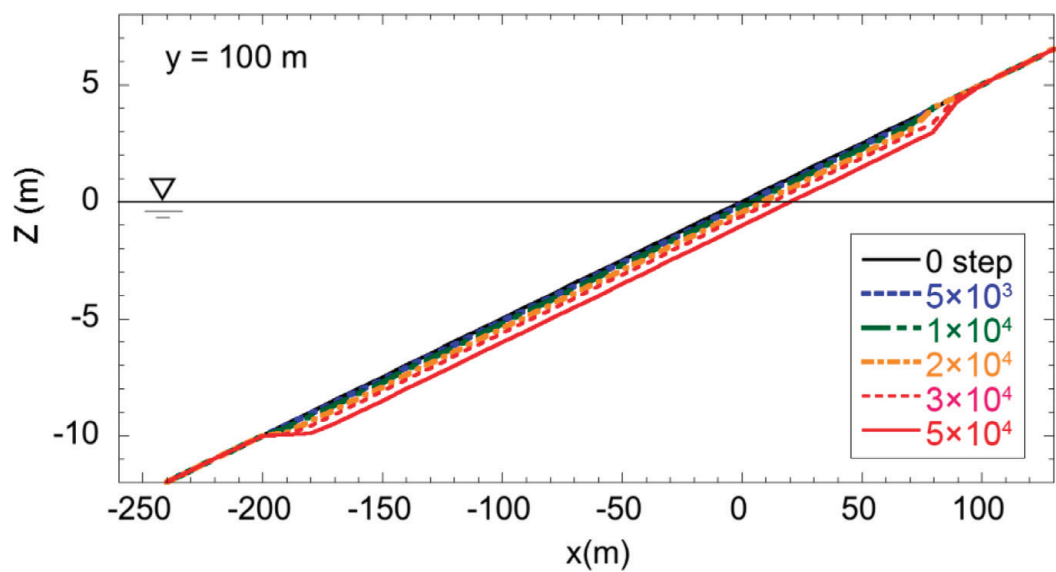

Figure 31.
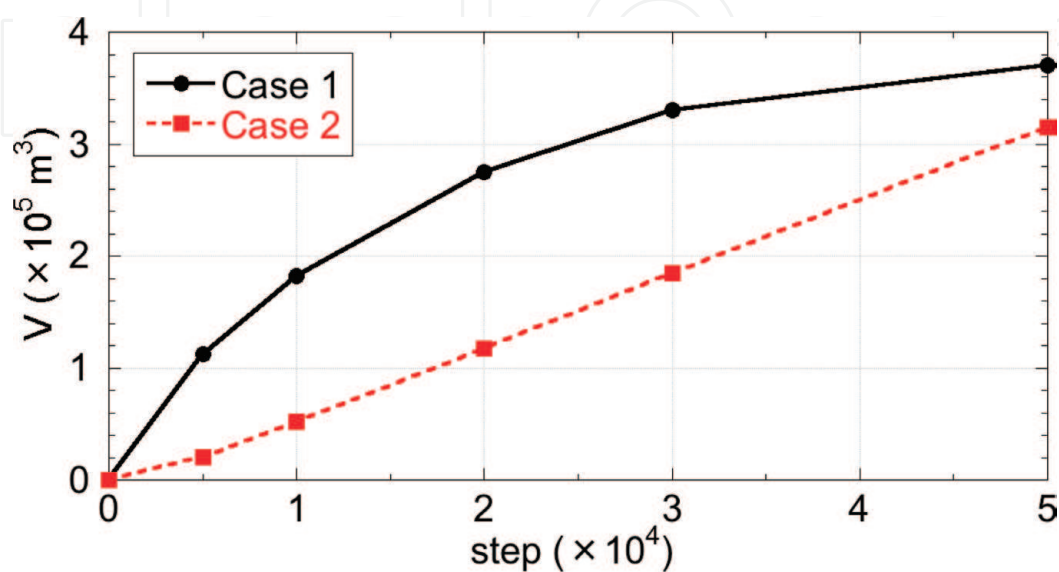*Changes in longitudinal profiles transect y = 100 m.*

Figure 32.
Change in sand volume accumulated inside port in Cases 1 and 2.

accumulated inside the port. At the initial stage, the rate of sand deposition in Case 1 without a jetty was very rapid compared with that in Case 2, but the difference between two cases decreased with time.

7. Conclusions

In Chapter 3, beach changes when groynes, detached breakwaters, and an oblique breakwater were constructed on a coast with parallel contours were predicted using the Types 1 and 2 BG model together with the prediction of the beach changes when offshore sand mining was carried out. The Types 1 and 2 BG model became a useful tool to solve these beach changes, which were frequently encountered in practical engineering. The Type 2 BG model that was employed in the present study was successfully used for the prediction of lakeshore changes associated with the extension of an offshore breakwater [6], and the prediction of the beach changes caused by not only the imbalance in longshore sand transport but also ground subsidence on south Kujūkuri Beach [7]. Such results can be referred in the original papers [6, 7].

As another application of the Type 2 BG model, the mechanism of sand deposition inside a fishing port was predicted in [8], and the Type 2 BG model was used for the prediction of beach changes triggered by the construction of a causeway on a coral reef coast on Miyako Island, Okinawa, in [9].

Author details

Takaaki Uda[1*], Masumi Serizawa[2] and Shiho Miyahara[2]

1 Public Works Research Center, Tokyo, Japan

2 Coastal Engineering Laboratory Co., Ltd., Tokyo, Japan

*Address all correspondence to: uda@pwrc.or.jp

IntechOpen

References

[1] Uda T. Japan's Beach Erosion–Reality and Future Measures. 2nd ed. Singapore: World Scientific; 2017. 530 p

[2] Serizawa M, Uda T, San-nami T, Furuike K. Three-dimensional model for predicting beach changes based on Bagnold's concept. In: Proceedings of 30th ICCE; 2006. pp. 3155-3167

[3] Serizawa M, Uda T, San-nami T, Furuike K, Ishikawa T. BG-model predicting three-dimensional beach changes based on Bagnold's concept and applications. In: Proceedings of 4th International Conference on Asian and Pacific Coasts 2007; 2007. pp. 1165-1179

[4] Ozasa H, Brampton AH. Model for predicting the shoreline evolution of beaches backed by seawalls. Coastal Engineering. 1980;**4**:47-64

[5] Uda T, Kawano S. Development of a predictive model of contour line change due to waves. In: Proceedings of JSCE, No. 539/II-35; 1996. pp. 121-139. (in Japanese)

[6] Uda T. Numerical simulation of formation of cuspate foreland behind an offshore breakwater built in a lake. In: 8th International Conference on Asian and Pacific Coasts (APAC 2015), Procedia Engineering. Vol. 116; 2015. pp. 478-485

[7] Uda T, Yoshida R, Todoroki T. Beach changes triggered by imbalance of longshore sand transport and ground subsidence on south Kujukuri Beach. In: Coastal Sediments'15, CD-Rom, No. 34; 2015. pp. 1-14

[8] Ohki Y, Uda T, Miyahara S, Serizawa M, San-nami T, Sumita A. Analysis of mechanism of sand deposition inside a fishing port using BG model. In: Proceedings of the 7th International Conference on Asian and Pacific Coasts 2013; 2013. pp. 32-39

[9] Uda T, Gibo M, Ishikawa M, Miyahara S, San-nami T, Serizawa M. Change in carbonate beach triggered by construction of a bridge on Irabu Island and its simulation using BG model. In: Proceedings of the 7th International Conference on Asian and Pacific Coasts 2013; 2013. pp. 24-31